

Persistent Test-time Adaptation in Recurring Testing Scenarios

Trung-Hieu Hoang¹ Duc Minh Vo² Minh N. Do¹

¹Department of Electrical and Computer Engineering, University of Illinois at Urbana-Champaign, USA

²The University of Tokyo, Japan

{hthieu, minhdo}@illinois.edu,

vmduc@nlab.ci.i.u-tokyo.ac.jp

Abstract

Current test-time adaptation (TTA) approaches aim to adapt to environments that change continuously. Yet, it is unclear whether TTA methods can remain their adaptability over prolonged periods. To answer this question, we introduce a diagnostic setting - **recurring TTA** where environments not only change but also recur over time, creating an extensive data stream. This setting allows us to examine the error accumulation of TTA models, in the most basic scenario, when they are regularly exposed to previous testing environments. Furthermore, we simulate a TTA process on a simple yet representative ϵ -perturbed **Gaussian Mixture Model Classifier**, deriving theoretical insights into the dataset- and algorithm-dependent factors contributing to gradual performance degradation. Our investigation leads us to propose **persistent TTA (PeTTA)**, which senses when the model is diverging towards collapse and adjusts the adaptation strategy, striking a balance between the dual objectives of adaptation and model collapse prevention. The supreme stability of PeTTA over existing approaches, in the face of lifelong TTA scenarios, has been demonstrated over comprehensive experiments on various benchmarks. The code is available at <https://github.com/hthieu166/petta>.

1. Introduction

Machine learning (ML) models have demonstrated significant achievements in various areas [18, 23, 36, 45]. Still, they are inherently susceptible to distribution-shift [6, 13, 21, 44, 46] (also known as the divergence between the training and testing environments), leading to a significant degradation in model performance. The ability to deviate from the conventional testing setting appears as a crucial aspect in boosting ML models' adaptability when confronted with a new testing environment that has been investigated [14, 29, 50]. Among domain generalization methods [1, 24, 55], test-time adaptation (TTA) takes the most challenging yet rewarding path that leveraging unlabeled

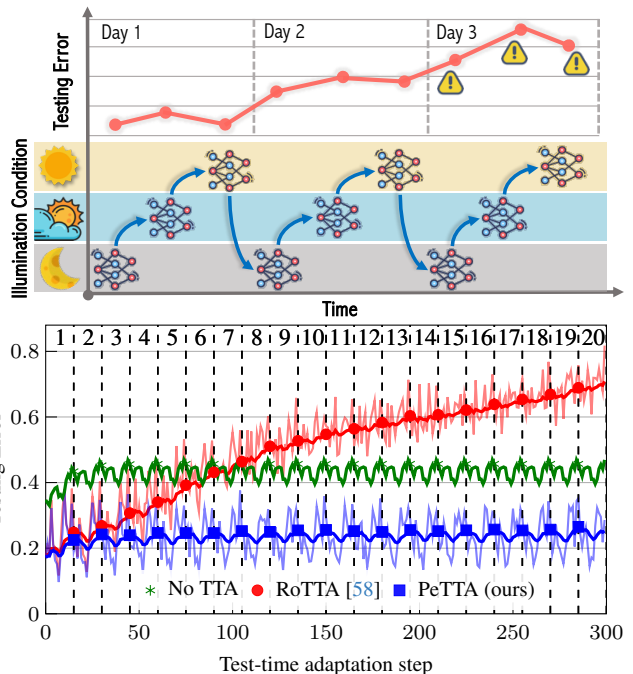


Figure 1. *Episodic Test-time Adaptation (TTA)*. (top) Testing environments may change episodically and preserving adaptability when visiting the same testing condition is not guaranteed in most cases. (bottom) The testing error of RoTTA [58] progressively raises (performance degradation) and exceeds the error of the source model (no TTA) while our PeTTA demonstrates its stability when adapting to the test set of CIFAR-10-C [19] 20 times. The shaded lines in the background represent the testing error on each domain and the bold lines denote the running mean. For clarity, only the running mean of the source model is shown.

data available at test time for self-supervised adaptation prior to the final inference [8, 37, 39, 54, 56].

Early TTA studies have concentrated on a simply ideal adaptation scenario where the test samples come from a fixed single domain [37, 39, 54]. As a result, such an assumption is far from the ever-changing and complex testing environments. To confront continually changing environments [12, 56], Yuan *et al.* [58] proposed a practical TTA scenario where distribution changing and correlative sam-

pling occur [15] simultaneously. Though practical TTA is more realistic than previous assumptions, it still assumes that any environment only appears once in the data stream which does not hold true. Taking a surveillance camera as an example, it might accommodate varying lighting conditions recurringly day after day (Fig. 1-top). Importantly, we hypothesize that the recurring of those conditions may reveal the error accumulation phenomenon in TTA, resulting in performance degradation over a long period. To verify our hypothesis, we simulate an recurring testing environment and observe the increasing error rate by recurringly adapting to the test set of CIFAR-10-C [19] multiple times. We showcase the testing error of RoTTA [58] after 20 cycles of adaptation in Fig. 1-bottom. As expected, RoTTA can successfully adapt and deliver encouraging outcomes within the first few passes. However, this advantage does not last long as our study reveals a significant problem: *TTA approaches in this setting may experience severe and persistent degradation in performance*. Consequently, the testing error of RoTTA gradually escalates over time and quickly surpasses the model without adaptation. This confirms the risk of TTA deployment in our illustrative scenario, as an algorithm might work well in the first place and gradually degenerate. Therefore, ensuring sustainable quality is crucial for real-world applications, particularly because testing environments often display an recurring nature.

This study examines whether the adaptability of a TTA algorithm persists over an extended testing stream. Specifically, in the most basic scenario, where the model returns to a previously encountered testing environment after undergoing various adjustments. We thus propose a more general testing scenario than the practical TTA [58], namely *recurring TTA*, where the environments change gradually and recur in a correlated manner over time. We first examine a simulation with the ϵ -perturbed Gaussian Mixture Model Classifier (ϵ -GMMC) on a synthesized dataset and derive the theoretical analysis to confirm the case and shed light to address similar problems in deep neural networks. The analysis provides hints for reasoning the success of many recent robust continual TTA approaches [12, 15, 56, 58] and leading us to propose an effective baseline to avoid performance degradation, namely *Persistent TTA (PeTTA)*. PeTTA continuously monitors the chance of collapsing and adjusts the adaptation strategy on the fly, striking a balance between the two objectives: *adaptation* and *preventing collapse*. Our contributions are as follows:

- First, this work *proposes a new testing scenario - recurring TTA*, a simple yet sufficient setup for diagnosing the overlooked *gradual performance degradation* of TTA.
- Second, we formally *define the phenomenon of TTA collapsing and undertake a theoretical analysis* on an ϵ -GMMC, shedding light on dataset-dependent and algorithm-dependent factors that contribute to the error

accumulation during TTA processes.

- Third, we *introduce persistent TTA (PeTTA)* - a simple yet effective adaptation scheme that surpasses all baseline models and demonstrates a persisting performance.

2. Related Work

Towards Robust and Practical TTA. While forming the basis, early single-target TTA approaches [32, 37, 39, 50, 54] is far from practice. Observing the dynamic of many testing environments, a continual TTA setting is proposed where an ML model continuously adapts to a sequence of multiple shifts [35, 56]. Meanwhile, recent studies [7, 15] point out that the category distribution realistic streams is highly temporally correlated. Towards real-world TTA setting, Yuan *et al.* [58] launch the *practical TTA* which considers the simultaneous occurrence of the two challenges.

For a robust and gradual adaptation, an update via the mean teacher [52] mechanism is exploited in many continual TTA algorithms [12, 22, 56, 58]. To moderate the temporally correlated test stream, common approaches utilize a small memory bank for saving a category-balanced subset of testing samples [15, 58], inspired by the replay methods [2, 48] to avoid forgetting in the task of continual learning [3, 11, 33]. Our study emphasizes another perspective: beyond a supreme performance, a desirable TTA should also *sustain it for an extended duration*.

Temporal Performance Degradation. By studying the quality of various ML models across multiple industry applications [53, 57] the issue of AI “aging” with the temporal model degradation progress, even with data coming from a stable process has been confirmed. In TTA, the continuous changes of model parameters through gradient descent aggravate the situation, as also noticed in [43]. Apart from observation, we attempt to investigate and provide *theoretical* insights towards the mechanism of this phenomenon.

Accumulated Errors in TTA. In TTA, the issue of accumulated error has been briefly acknowledged. Previous works strive to avoid drastic changes to model parameters as a good practice. Up to some degree, it helps to avoid performance degradation. Nevertheless, it is still *unclear whether their effectiveness truly eliminates the risk*. To preserve in-distribution performance, regularization [27, 38] or replaying [12] have been used. Other studies explore reset (recovering the source model) [43, 56], periodically or upon the running entropy loss approaches a threshold [39]. Unfortunately, knowledge accumulated in the preceding steps will vanish, and a bad heuristic choice of threshold or period leads to highly frequent model resets. Noteworthy, tuning those hyper-parameters is exceedingly difficult due to the unavailability of the validation set [59]. LAME [7] suggests a post-processing step for adaptation (without updating the parameters). This approach, however, still limits the knowledge accumulation. Our PeTTA is *reset-free* by achieving an adaptable continual test-time training.

3. Background

Test-time Adaptation (TTA). A TTA algorithm operates on an ML classifier $f_t : \mathcal{X} \rightarrow \mathcal{Y}$ with parameter $\theta_t \in \Theta$ (parameter space) gradually changing over time ($t \in \mathcal{T}$) that maps an input image $x \in \mathcal{X}$ to a category (label) $y \in \mathcal{Y}$. Let the capital letters $(X_t, Y_t) \in \mathcal{X} \times \mathcal{Y}$ denote a pair of *random variables* with the joint distribution $P_t(x, y) \in \mathcal{P}_d, t \in \mathcal{T}$. Here, \mathcal{P}_d belongs to collection of D sets of testing scenarios (domains) $\{\mathcal{P}_d\}_{d=1}^D$. The covariate shift [44] is assumed: $P_t(x)$ and $P_{t'}(x)$ could be different but $P_t(y|x) = P_{t'}(y|x)$ holds $\forall t \neq t'$. At $t = 0$, θ_0 is initialized by a supervised model trained on $P_0 \in \mathcal{P}_0$ (source dataset). The model then explores an online stream of testing data. For each $t > 0$, it receives X_t (typically in form of a batch of N_t testing samples) for adapting itself $f_{t-1} \rightarrow f_t$ before making the final prediction $f_t(X_t)$.

TTA with Mean Teacher Update. To achieve a stable optimization process, the main (*teacher*) model f_t are updated indirectly through a *student* model with parameters θ'_t [12, 15, 52, 54, 58]. At first, the teacher model in the previous step introduces a *pseudo label* [28] \hat{Y}_t for each X_t :

$$\hat{Y}_t = f_{t-1}(X_t). \quad (1)$$

With a classification loss \mathcal{L}_{CLS} (e.g., cross-entropy [16]), and a model parameters regularizer \mathcal{R} , the student model is first updated with a generic optimization operator Optim , followed by an exponential moving average (EMA) update of the teacher model parameter θ_{t-1} :

$$\theta'_t = \underset{\theta' \in \Theta}{\text{Optim}} \mathbb{E}_{P_t} \left[\mathcal{L}_{\text{CLS}} \left(\hat{Y}_t, X_t; \theta' \right) \right] + \lambda \mathcal{R}(\theta'), \quad (2)$$

$$\theta_t = (1 - \alpha)\theta_{t-1} + \alpha\theta'_t, \quad (3)$$

with $\alpha \in (0, 1)$ - the update rate of EMA, $\lambda \in \mathbb{R}^+$ - weighting coefficient of regularization term are hyper-parameters.

Practical TTA. In practical TTA [58], two characteristics of the aforementioned distribution of data stream are noticeable. Firstly, P_t 's can be partitioned by t_d 's in which $\{P_t\}_{t=t_d-1}^{t_d} \subset \mathcal{P}_d$. Here, each partition of consecutive steps follows the same underlying distribution which will *change continually through D domains* [56] ($\mathcal{P}_1 \rightarrow \mathcal{P}_2 \cdots \rightarrow \mathcal{P}_D$). Secondly, the category distribution in each testing batch is *temporally correlated* [15]. This means within a batch, a small subset of categories is dominant over others, making the marginal distribution $P_t(y) = 0, \forall y \notin \mathcal{Y}_t \subset \mathcal{Y}$ even though the category distribution over all batches are balanced. Optimizing under this low intra-batch diversity ($|\mathcal{Y}_t| \ll |\mathcal{Y}|$) situation can slowly degenerate the model [7].

4. Recurring TTA and Theoretical Analysis

This section conducts a theoretical analysis on a concrete failure case of a simple TTA model. The results presented at the end of Sec. 4.2 will elucidate the factors contributing to the collapse (Sec. 4.1), explaining existing good practices

(Sec. 4.3) and give insights into potential solutions (Sec. 5).

4.1. Recurring TTA and Model Collapse

Recurring TTA. To study the gradual performance degradation (or model collapse), we propose a *new testing scenario* based on practical TTA. Conducting a single pass through D distributions, as done in earlier studies [56, 58], may not effectively identify the degradation. To promote consistency, our recurring TTA performs *revisiting the previous distributions K times* to compare the incremental error versus the previous visits. For example, a sequence with $K = 2$ could be $\mathcal{P}_1 \rightarrow \mathcal{P}_2 \rightarrow \cdots \rightarrow \mathcal{P}_D \rightarrow \mathcal{P}_1 \rightarrow \mathcal{P}_2 \rightarrow \cdots \rightarrow \mathcal{P}_D$. Appdx. C extends our justifications on constructing recurring TTA.

Definition 1 (Model Collapse). A model is said to be collapsed from step $\tau \in \mathcal{T}, \tau < \infty$ if there exists a non-empty subset of categories $\tilde{\mathcal{Y}} \subset \mathcal{Y}$ such that $\Pr\{Y_t \in \tilde{\mathcal{Y}}\} > 0$ but the marginal $\Pr\{\hat{Y}_t \in \tilde{\mathcal{Y}}\}$ converges to zero in probability:

$$\lim_{t \rightarrow \tau} \Pr\{\hat{Y}_t \in \tilde{\mathcal{Y}}\} = 0.$$

Here, upon collapsing, a model tends to *ignore* all categories in $\tilde{\mathcal{Y}}$. As it is irrecoverable once collapsed, the only remedy would be resetting all parameters back to θ_0 .

4.2. Simulation of Failure and Theoretical Analysis

Collapsing behavior varies across datasets and the adaptation processes. Formally studying this phenomenon on a particular real dataset and a TTA algorithm is challenging. Therefore, we propose a theoretical analysis on ϵ -perturbed binary Gaussian Mixture Model Classifier (ϵ -GMMC) that shares the typical characteristics *by construction* and demonstrates the *same collapsing pattern* in action (Sec. 6.1) as observed on real continual TTA processes (Sec. 6.3).

Simulated Testing Stream. Observing a testing stream with $(X_t, Y_t) \in \mathcal{X} \times \mathcal{Y} = \mathbb{R} \times \{0, 1\}$ and the underlying joint distribution $P_t(x, y) = p_{y,t} \cdot \mathcal{N}(x; \mu_y, \sigma_y^2)$. The main task is predicting X_t was sampled from cluster 0 or 1 (negative or positive). Conveniently, let $p_{y,t} \triangleq P_t(y) = \Pr(Y_t = y)$ and $\hat{p}_{y,t} \triangleq \Pr(\hat{Y}_t = y)$ be the marginal distribution of the true label Y_t and pseudo label \hat{Y}_t .

GMMC and TTA. GMMC first implies an *equal prior* distribution by construction which is desirable for the actual TTA algorithms (e.g., category-balanced sampling strategies in [15, 58]). Thus, it simplifies f_t into a maximum likelihood estimation $f_t(x) = \arg\max_{y \in \mathcal{Y}} \Pr(x|y; \theta_t)$ with $\Pr(x|y; \theta_t) = \mathcal{N}(x; \hat{\mu}_{y,t}, \hat{\sigma}_{y,t}^2)$. The goal is estimating a set of parameters $\theta_t = \{\hat{\mu}_{y,t}, \hat{\sigma}_{y,t}^2\}_{y \in \mathcal{Y}}$. A perfect classifier $\theta_0 = \{\mu_y, \sigma_y^2\}_{y \in \mathcal{Y}}$ is initialized at $t = 0$. For the consecutive steps, the simplicity of GMMC allows solving the Optim (for finding θ'_t , Eq. 2) perfectly by computing the

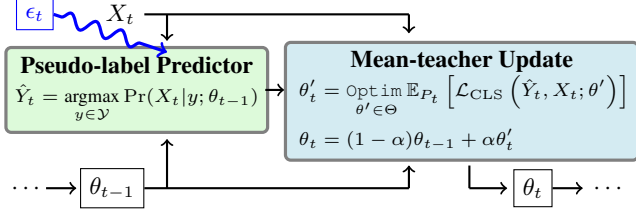


Figure 2. Diagram of our proposed ϵ -perturbed binary Gaussian Mixture Model Classifier (ϵ -GMMC), imitating a regular continual TTA algorithm for theoretical analysis. Two main components include a predictor for producing pseudo-label \hat{Y}_t (Eq. 1), and a mean teacher update (Eqs. 2, 3). The predictor is perturbed for retaining a false negative rate of ϵ_t to simulate undesirable effects of the testing stream in TTA, making ϵ -GMMC prone to collapse.

empirical mean and variance of new samples, approximating \mathbb{E}_{P_t} . The mean teacher update (Eq. 3) for GMMC is:

$$\hat{\mu}_{y,t} = \begin{cases} (1 - \alpha)\hat{\mu}_{y,t-1} + \alpha\mathbb{E}_{P_t}[X_t|\hat{Y}_t] & \text{if } \hat{Y}_t = y \\ \hat{\mu}_{y,t-1} & \text{otherwise} \end{cases} \quad (4)$$

The update of $\hat{\sigma}_{y,t}^2$ is similar. $\hat{Y}_t = f_{t-1}(X_t)$ can be interpreted as a *pseudo label* (Eq. 1).

ϵ -GMMC. Severe distribution shifts or low intra-batch category diversity of recurring TTA/practical TTA both result in an increase in the error rate of the predictor. Instead of directly modeling the dynamic changes of $p_{y,t}$ (which can be complicated depending on the dataset), we study an ϵ -perturbed GMMC (ϵ -GMMC), where $p_{y,t}$ is assumed to be static (defined below) and the pseudo-label predictor of this model is perturbed to simulate undesirable effects of the testing stream on the predictor. Two kinds of errors appear in a binary classifier [4]. Let

$$\epsilon_t = \Pr\{Y_t = 1 | \hat{Y}_t = 0\} \quad (5)$$

be the false negative rate (FNR) of the model at step t . Without loss of generality, we study the *increasing type II collapse of ϵ -GMMC*. By flipping the true positive pseudo labels in simulation, an FNR of ϵ_t is maintained (Fig. 2).

Assumption 1 (Static Data Stream). *The marginal distribution of the true label follows the same Bernoulli distribution $\text{Ber}(p_0)$: $p_{0,t} = p_0$, $(p_{1,t} = p_1 = 1 - p_0)$, $\forall t \in \mathcal{T}$.*

Lemma 1 (Increasing FNR). *Under Assumption 1, a binary ϵ -GMMC would collapsed (Def. 1) with $\lim_{t \rightarrow \tau} \hat{p}_{1,t} = 0$ (or $\lim_{t \rightarrow \tau} \hat{p}_{0,t} = 1$, equivalently) if and only if $\lim_{t \rightarrow \tau} \epsilon_t = p_1$.*

Lemma 1 states the negative correlation between $\hat{p}_{1,t}$ and ϵ_t . Unsurprisingly, towards the collapsing point where all predictions are zeros, the FNR also increases at every step and eventually reaches the highest possible FNR of p_1 .

Lemma 2 (ϵ -GMMC After Collapsing). *For a binary ϵ -GMMC model, with Assumption 1, if $\lim_{t \rightarrow \tau} \hat{p}_{1,t} = 0$ (collapsing), the cluster 0 in GMMC converges in distribution to a*

single-cluster GMMC with parameters:

$$\mathcal{N}(\hat{\mu}_{0,t}, \hat{\sigma}_{0,t}^2) \xrightarrow{d} \mathcal{N}(p_0\mu_0 + p_1\mu_1, p_0\sigma_0^2 + p_1\sigma_1^2 + p_0p_1(\mu_0 - \mu_1)^2).$$

Lemma 2 states the resulting ϵ -GMMC after collapsing. Cluster 0 now covers the whole data distribution (and assigning label 0 for all samples). Furthermore, *collapsing happens when $\hat{\mu}_{0,t}$ moves toward μ_1* . We next investigate the factors and conditions for this undesirable convergence.

Theorem 1 (Convergence of ϵ -GMMC). *For a binary ϵ -GMMC model, with Assumption 1, let the distance from $\hat{\mu}_{0,t}$ toward μ_1 is $d_t^{0 \rightarrow 1} = |\mathbb{E}_{P_t}[\hat{\mu}_{0,t}] - \mu_1|$, then:*

$$d_t^{0 \rightarrow 1} - d_{t-1}^{0 \rightarrow 1} \leq \alpha \cdot p_0 \cdot \left(|\mu_0 - \mu_1| - \frac{d_{t-1}^{0 \rightarrow 1}}{1 - \epsilon_t} \right).$$

From Thm. 1, we observe that the distance $d_t^{0 \rightarrow 1}$'s converges (also indicating the convergence to the distribution in Lemma 2) if $d_t^{0 \rightarrow 1} < d_{t-1}^{0 \rightarrow 1}$. The model collapse happens when this condition holds for a sufficiently long period.

Corollary 1 (A Condition for ϵ -GMMC Collapse). *With fixed p_0 , α , μ_0 , μ_1 , ϵ -GMMC is collapsed if there exists a sequence of $\{\epsilon_t\}_{\tau - \Delta_\tau}^\tau$ ($\tau \geq \Delta_\tau > 0$) such that:*

$$p_1 \geq \epsilon_t > 1 - \frac{d_{t-1}^{0 \rightarrow 1}}{|\mu_0 - \mu_1|}, \quad t \in [\tau - \Delta_\tau, \tau].$$

Corollary 1 introduces a condition ϵ -GMMC collapse. Here, ϵ_t 's are non-decreasing, following that $\lim_{t \rightarrow \tau} \epsilon_t = p_1$.

Remarks. Thm. 1 concludes two sets of factors contributing to collapse: (i) *data-dependent factors*: the prior data distribution (p_0), the nature difference between two categories ($|\mu_0 - \mu_1|$); and (ii) *algorithm-dependent factors*: the update rate (α), the FNR at each step (ϵ_t). ϵ -GMMC analysis sheds light on explaining model collapse on real datasets (Sec. 6.3), reasons the existing approaches (Sec. 4.3) and motivates the development of our baseline (Sec. 5).

4.3. Connection to Existing Solutions

Prior TTA algorithms have already incorporated implicit mechanisms to mitigate model collapse. We briefly discuss the rationale behind these effective strategies before introducing our solution to bolster the resilience of TTA.

Regularization Term for θ_t . Knowing that f_0 is always well-behaved, an attempt is restricting the divergence of θ_t from θ_0 , e.g. using $\mathcal{R}(\theta_t) \triangleq \|\theta_0 - \theta_t\|_2^2$ regularization [38]. The key idea is introducing a penalty term to avoid an extreme divergence as happening in Thm. 1.

Memory Bank for Harmonizing $P_t(x)$. Upon receiving X_t , samples in this batch are selectively updated to a memory bank \mathcal{M} (which already contains a subset of some instances of $X_{t'}$, $t' < t$ in the previous steps). By keeping a

balanced number of samples from each category, distribution $P_t^{\mathcal{M}}(y)$ of samples in \mathcal{M} is expected to have less zero entries than $P_t(y)$, making the optimization step over $P_t^{\mathcal{M}}$ more desirable. From Thm. 1, \mathcal{M} moderates the extreme value of the category distribution (p_0 term) which typically appears on batches with low intra-batch category diversity.

5. Persistent Test-time Adaptation (PeTTA)

Now we introduce our *Persistent TTA (PeTTA)* approach. Further inspecting Thm. 1, while ϵ_t (Eq. 5) is not computable without knowing the true labels, the measure of divergence from the initial distribution (analogously to $d_{t-1}^{0 \rightarrow 1}$ term) can provide hints to fine-tune the adaptation process.

Key Idea. A proper adjustment toward the TTA algorithm can *break the chain of increasing ϵ_t 's* in Corollary 1 to prevent the model collapse. In the mean teacher update, the larger value of λ (Eq. 2) prioritizes the task of preventing collapse on one hand but also limits its adaptability to the new testing environment. Meanwhile, α (Eq. 3) controls the weight on preserving versus changing the model from the previous step. Drawing inspiration from the exploration-exploitation tradeoff [25, 47] encountered in reinforcement learning [51], we introduce a mechanism for *adjusting λ and α on the fly, balancing between the two primary objectives: adaptation and preventing model collapse*. Our strategy is prioritizing collapse prevention (increasing λ) and preserving the model from previous steps (decreasing α) when there is a significant deviation from θ_0 .

Different from [38, 56, 58], where λ and α were selected by hyper-parameter tuning and kept constant over time. This is less than the ideal approach in TTA, where a testing environment might vary and the validation set is unavailable [59]. Furthermore, Thm. 1 suggests the rate of convergence quickly escalates when ϵ_t increases. Hence, constant values for λ, α might be insufficient to stop the collapsing.

Sensing the Divergence of θ_t . We first equip PeTTA with a mechanism for *measuring its divergence from θ_0* . Noticed that with $f_t(\mathbf{x}) = \operatorname{argmax}_{y \in \mathcal{Y}} \Pr(y|\mathbf{x}; \theta_t)$, we can decompose $\Pr(y|\mathbf{x}; \theta_t) = [h(\phi_{\theta_t}(\mathbf{x}))]_y$, with $\phi_{\theta_t}(\cdot)$ is a θ_t -parameterized deep feature extractor followed by a *fixed* classification head (a linear and softmax layer) $h(\cdot)$. The operator $[\cdot]_y$ extracts the y^{th} component of a vector.

Since $h(\cdot)$ remains unchanged, instead of comparing the divergence in the parameter space (Θ) or between the output probability $\Pr(y|\mathbf{x}; \theta_t)$ and $\Pr(y|\mathbf{x}; \theta_0)$, we suggest an *inspection over the feature embedding space* that preserves a *maximum amount of information* in our case (data processing inequality [9]). Inspired by [30] and under Gaussian assumption, the Mahalanobis distance of the first moment of the feature embedding vectors is compared. Let $\mathbf{z} = \phi_{\theta_t}(\mathbf{x})$, we keep track of a collection of the running mean of feature vector \mathbf{z} : $\{\hat{\boldsymbol{\mu}}_t^y\}_{y \in \mathcal{Y}}$ in which $\hat{\boldsymbol{\mu}}_t^y$ is EMA

updated with vector \mathbf{z} if $f_t(\mathbf{x}) = y$. The divergence of θ_t at step t , evaluated on class y is defined as:

$$\gamma_t^y = 1 - \exp\left(-(\hat{\boldsymbol{\mu}}_t^y - \boldsymbol{\mu}_0^y)^T (\boldsymbol{\Sigma}_0^y)^{-1} (\hat{\boldsymbol{\mu}}_t^y - \boldsymbol{\mu}_0^y)\right), \quad (6)$$

where $\boldsymbol{\mu}_0^y$ and $\boldsymbol{\Sigma}_0^y$ are the pre-computed empirical mean and covariant matrix of feature vectors in the training set (P_0). The covariant matrix here is diagonal for simplicity. In practice, without directly accessing the training set, we assume a small set of unlabeled samples can be drawn from the source distribution for empirically computing these values (visit Appdx. D.4 for further details).

Here, we implicitly expect the independence of each entry in \mathbf{z} and TTA approaches *learn to align feature vectors of new domains back to the source domain (P_0)*. Therefore, the accumulated statistics of these feature vectors at each step should be concentrated near the vectors of the initial model. The value of $\gamma_t^y \in [0, 1]$ is close to 0 when $\theta_t = \theta_0$ and increases exponentially as $\hat{\boldsymbol{\mu}}_t^y$ diverging from $\boldsymbol{\mu}_0^y$.

Adaptive Regularization and Model Update. Utilizing γ_t^y derived in Eq. 6, a pair of (λ_t, α_t) is chosen at each step:

$$\begin{aligned} \bar{\gamma}_t &= \frac{1}{|\hat{\mathcal{Y}}_t|} \sum_{y \in \hat{\mathcal{Y}}_t} \gamma_t^y, & \hat{\mathcal{Y}}_t &= \left\{ \hat{Y}_t^{(i)} \mid i = 1, \dots, N_t \right\}; \\ \lambda_t &= \bar{\gamma}_t \cdot \lambda_0, & \alpha_t &= (1 - \bar{\gamma}_t) \cdot \alpha_0, \end{aligned} \quad (7)$$

where α_0, λ_0 are initial values; $\hat{\mathcal{Y}}_t$ is a set of unique pseudo labels in a testing batch ($\hat{Y}_t^{(i)}$ is the i^{th} realization of \hat{Y}_t).

Anchor Loss. Penalizing the divergence with regular vector norms in high-dimensional space (Θ) is insufficient (curse of dimensionality [5, 49]), especially with a large model and limited samples. *anchor loss* \mathcal{L}_{AL} is proposed to further nail down the similarity between f_t and f_0 in the output probability space [12, 31]:

$$\mathcal{L}_{\text{AL}}(X_t; \theta) = - \sum_{y \in \mathcal{Y}} \Pr(y|X_t; \theta_0) \log \Pr(y|X_t; \theta), \quad (8)$$

which is equivalent to minimizing the KL divergence $D_{\text{KL}}(\Pr(y|X_t; \theta_0) \parallel \Pr(y|X_t; \theta))$.

Persistent TTA. Having all the ingredients, we design our approach, PeTTA, following the convention setup of the mean teacher update, with the category-balanced memory bank and the robust batch normalization layer from [58]. Appdx. D.1 introduces the pseudo code of PeTTA. For \mathcal{L}_{CLS} , we either adopt the self-training scheme [12] or the regular cross-entropy [16]. With $\mathcal{R}(\theta)$, cosine similarity or L2 distance are both valid metrics for measuring the distance between θ and θ_0 in the parameter space. Fisher regularizer coefficient [27, 38] can also be used, optionally. To sum up, the teacher model update of PeTTA is an *elaborated version* of EMA with λ_t, α_t (Eq. 7) and \mathcal{L}_{AL} (Eq. 8):

$$\begin{aligned} \theta'_t &= \operatorname{Opt}_{\theta' \in \Theta} \mathbb{E}_{P_t} \left[\mathcal{L}_{\text{CLS}}(\hat{Y}_t, X_t; \theta') + \mathcal{L}_{\text{AL}}(X_t; \theta') \right] + \lambda_t \mathcal{R}(\theta') \\ \theta_t &= (1 - \alpha_t) \theta_{t-1} + \alpha_t \theta'_t. \end{aligned}$$

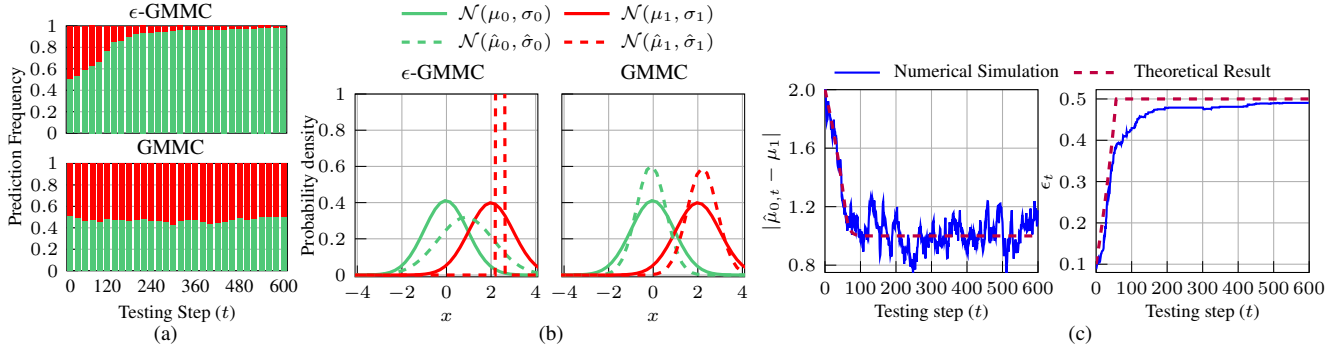


Figure 3. Simulation result on ϵ -perturbed Gaussian Mixture Model Classifier (ϵ -GMMC) and GMMC (perturbed-free). (a) Histogram of model predictions through time. A similar prediction frequency pattern is observed on CIFAR-10-C (Fig. 4a-top). (b) The probability density function of the two clusters after convergence versus the true data distribution. The initial two clusters of ϵ -GMMC collapsed into a single cluster with parameters stated in Lemma 2. In the perturbed-free, GMMC converges to the true data distribution. (c) Distance toward μ_1 ($|\mathbb{E}_{P_t}[\hat{\mu}_{0,t}] - \mu_1|$) and false-negative rate (ϵ_t) in simulation coincides with the result in Thm. 1 (with ϵ_t following Corollary 1).

6. Experimental Results

6.1. ϵ -GMMC Simulation Result

Setup. A total of 6000 samples from two Gaussian distributions: $\mathcal{N}(\mu_0 = 0, \sigma_0^2 = 1)$ and $\mathcal{N}(\mu_1 = 2, \sigma_1^2 = 1)$ with $p_0 = p_1 = \frac{1}{2}$ are synthesized and gradually released in a batch of $B = 10$ samples. For evaluation, an independent set of 2000 samples following the same distribution is used for computing the prediction frequency, and the false negative rate (FNR). ϵ -GMMC update follows Eq. 4 with $\alpha = 5e^{-2}$. To simulate model collapse, the predictor is intercepted and 10% of the true-positive pseudo labels at each testing step are randomly flipped (Corollary 1).

Simulation Result. In action, both the likelihood of predicting class 0 (Fig. 3a-top) and the ϵ_t (Eq. 5) (Fig. 3c-right, solid line) gradually increases over time as expected (Lemma 1). After collapsing, ϵ -GMMC merges the two initial clusters, resulting in a single one (Fig. 3b-left) with parameters that match Lemma 2. The distance from $\hat{\mu}_{0,t}$ (initialized at μ_0) towards μ_1 converges (Fig. 3c-left, solid line), coincided with the analysis in Thm. 1 when ϵ_t is chosen following Corollary 1 (Fig. 3c, dashed line). GMMC (perturbed-free) stably produces accurate predictions (Fig. 3a-bottom) and approximates the true data distribution (Fig. 3b-right). The simulation empirically validates our analysis (Sec. 4.2), confirming the vulnerability of TTA models when the pseudo labels are inaccurately estimated.

6.2. Setup - Benchmark Datasets

Datasets. We benchmark the performance on *four* TTA classification tasks. Specifically, CIFAR10 \rightarrow CIFAR10-C, CIFAR100 \rightarrow CIFAR100-C, and ImageNet \rightarrow ImageNet-C [19] are three classification on corrupted images (corruption level 5, the most severe) tasks. Additionally, we incorporate DomainNet [42] with 126 categories from four domains for the task *real* \rightarrow *clipart*, *painting*, *sketch*.

Compared Methods. Besides PeTTA, the following algorithms are investigated: CoTTA [56], RMT [12], MECTA [22] with EATA [38] serving as the backbone method, and RoTTA [58]. Noteworthy, only RoTTA is specifically designed for the practical TTA setting while others fit the continual TTA setting in general. A parameter-free approach: LAME [7] and a reset-based approach (i.e., reverting the model to the source model after adapting to every 1,000 images): RDumb [43] are also included.

Recurring TTA. Following the practical TTA setup, multiple testing scenarios from each testing set will gradually change from one to another while the Dirichlet distribution $\text{Dir}(0.1)$ for CIFAR10-C and DomainNet, $\text{Dir}(0.01)$ for CIFAR100-C) generates category temporally correlated batches of data. For all experiments, we set the number of revisits $K = 20$ (times) as this number is sufficient to fully observe the gradual degradation on existing TTA baselines.

Implementation Details. We use PyTorch [41] for implementation. RobustBench [10] and torchvision [34] provide pre-trained source models. Hyper-parameter choices are kept as close as possible to the original selections of authors. Unless otherwise noted, for all PeTTA experiments, the EMA update rate for robust batch normalization [58] and feature embedding statistics is set to $5e^{-2}$; $\alpha_0 = 1e^{-3}$ and cosine similarity regularizer is used. On CIFAR10/100-C and ImageNet-C we use the self-training loss in [12] for \mathcal{L}_{CLS} and $\lambda_0 = 10$ while the regular cross-entropy loss [13] and $\lambda_0 = 1$ (severe domain shift requires prioritizing adaptability) are applied in DomainNet experiments.

6.3. Result - Benchmark Datasets

Recurring TTA Performance. Fig. 1-bottom presents the testing error on CIFAR-10-C in recurring TTA setting. RoTTA [58] exhibits promising performance in the first several visits but soon raises and eventually exceeds the

Table 1. Average classification error of the task CIFAR-10 \rightarrow CIFAR-10-C in *recurring TTA*. The lowest error is highlighted in **bold**, (*) Average error across 5 runs (different random seeds) is reported for PeTTA.

Method	Recurring TTA visit \rightarrow																				Avg
	1	2	3	4	5	6	7	8	9	10	11	12	13	14	15	16	17	18	19	20	
Source	43.5																				43.5
LAME [7]	31.1																				31.1
CoTTA [56]	82.2	85.6	87.2	87.8	88.2	88.5	88.7	88.7	88.9	88.9	89.2	89.2	89.2	89.1	89.2	89.2	89.1	89.3	89.3	88.3	
RMT [12]	77.5	76.9	76.5	75.8	75.5	75.5	75.4	75.4	75.5	75.3	75.5	75.6	75.5	75.5	75.7	75.6	75.7	75.6	75.7	75.8	
MECTA [22]	72.2	82.0	85.2	86.3	87.0	87.3	87.3	87.5	88.1	88.8	88.9	88.9	88.6	89.1	88.7	88.8	88.5	88.6	88.3	88.8	
RoTTA [58]	24.6	25.5	29.6	33.6	38.2	42.8	46.2	50.6	52.2	54.1	56.5	57.5	59.4	60.2	61.7	63.0	64.8	66.1	68.2	70.3	
RDumb [43]	31.1	32.1	32.3	31.6	31.9	31.8	31.8	31.9	31.9	32.1	31.7	32.0	32.5	32.0	31.9	31.6	31.9	31.4	32.3	32.4	
PeTTA (ours) (*)	24.3	23.0	22.6	22.4	22.4	22.5	22.3	22.5	22.8	22.8	22.6	22.7	22.7	22.9	22.6	22.7	22.6	22.8	22.9	23.0	

Table 2. Average classification error of the task ImageNet \rightarrow ImageNet-C in *recurring TTA* scenario.

Method	Recurring TTA visit \rightarrow																				Avg
	1	2	3	4	5	6	7	8	9	10	11	12	13	14	15	16	17	18	19	20	
Source	82.0																				82.0
LAME [7]	80.9																				80.9
CoTTA [56]	98.6	99.1	99.4	99.4	99.5	99.5	99.5	99.5	99.6	99.7	99.6	99.6	99.6	99.6	99.6	99.6	99.6	99.6	99.7	99.7	
RMT [12]	72.3	71.0	69.9	69.1	68.8	68.5	68.4	68.3	70.0	70.2	70.1	70.2	72.8	76.8	75.6	75.1	75.1	75.2	74.8	74.7	
MECTA [22]	77.2	82.8	86.1	87.9	88.9	89.4	89.8	89.9	90.0	90.4	90.6	90.7	90.7	90.8	90.8	90.9	90.8	90.8	90.7	90.8	
RoTTA [58]	68.3	62.1	61.8	64.5	68.4	75.4	82.7	95.1	95.8	96.6	97.1	97.9	98.3	98.7	99.0	99.1	99.3	99.4	99.5	99.6	
RDumb [43]	72.2	73.0	73.2	72.8	72.2	72.8	73.3	72.7	71.9	73.0	73.2	73.1	72.0	72.7	73.3	73.1	72.1	72.6	73.3	73.1	
PeTTA (ours) (*)	65.3	61.7	59.8	59.1	59.4	59.6	59.8	59.3	59.4	60.0	60.3	61.0	60.7	60.4	60.6	60.7	60.8	60.7	60.4	60.2	

source model (no TTA). The classification error of compared methods on CIFAR-10 \rightarrow CIFAR-10-C, and ImageNet \rightarrow ImageNet-C [19] tasks are shown in Tab. 1, and Tab. 2. Appdx. E.1 provides the results on the other two datasets. The observed performance degradation of CoTTA [56], RoTTA [58] *confirms the risk of error accumulation* for an extensive period. While RMT [12] and MECTA [22] remain stable, they failed to adapt to the temporally correlated test stream at the beginning, with a higher error rate than the source model. LAME [7] (parameter-free TTA) does not suffer from collapsing, but the accuracy is lagging behind since its performance is constrained by the source model, and knowledge acquisition is impossible [7, 58].

In average, PeTTA simultaneously *outperforms all baseline approaches* (including state-of-the-art RoTTA [58] and LAME [7]) and *persists across 20 visits* over the three datasets (see Fig. 1b-right, Fig. 4a-right for CIFAR-10-C visualization). As the degree of freedom for adaptation in PeTTA is more constrained, it takes a bit longer for adaptation but remains stable afterward. Fig. 4b-bottom exhibits the confusion matrix at the last visit with satisfactory accuracy. Noteworthy, selecting a precise reset frequency for RDumb [43] is challenging in practice (see Appdx. E.3), and this approach limits knowledge accumulation that could favor a higher performance as achieved by PeTTA. The supreme performance of PeTTA is also validated on Continuously Changing Corruption [43] scenario (Appdx. E.4) and when the order of domain shifts within each recurrence is shuffled (Appdx. C.3).

Collapsing Pattern. The rise in classification error (Fig 1-bottom) can be reasoned by the prediction frequency of

RoTTA [58] in an recurring TTA setting (Fig. 4a-top). Similar to ϵ -GMMC, the likelihood of receiving predictions on certain categories gradually increases and dominates the others. Further inspecting the confusion matrix of a collapsed model (Fig. 4b-left) reveals two major groups of categories are formed and a single category within each group represents all members, thereby becoming dominant. To see this, Fig. 4c-left simplifies the confusion matrix by only visualizing the top prone-to-misclassified pair of categories. Here, label *deer* is used for almost every living animal while *airplane* represents transport vehicles. The similarity between categories in the feature space of the source model (Fig. 4c-right) is correlated with the likelihood of being merged upon collapsing. As distance in feature space is analogous to $|\mu_0 - \mu_1|$ (Thm. 1), closer clusters are at a higher risk of collapsing. This explains and showcases that the collapsing behavior is predictable up to some extent.

6.4. Ablation Study

Effect of Each Component. Tab. 3 gives an ablation study on PeTTA. It is important to highlight that adding a regularization term alone with a fixed choice of λ, α not only fails to mitigate the phenomenon of model collapse but may also introduce a negative effect (rows 1-3). Within PeTTA, adopting the adaptive λ_t scheme alone (row 4) or in conjunction with either α_t or anchor loss \mathcal{L}_{AL} (rows 5-6) partially stabilizes the performance. Under the drastic domain shifts with a larger size of categories or model parameters (e.g., on CIFAR-100-C, DomainNet, ImageNet-C), restricting α_t adjustment limits the ability of PeTTA to stop undesirable updates while a common regularization term without

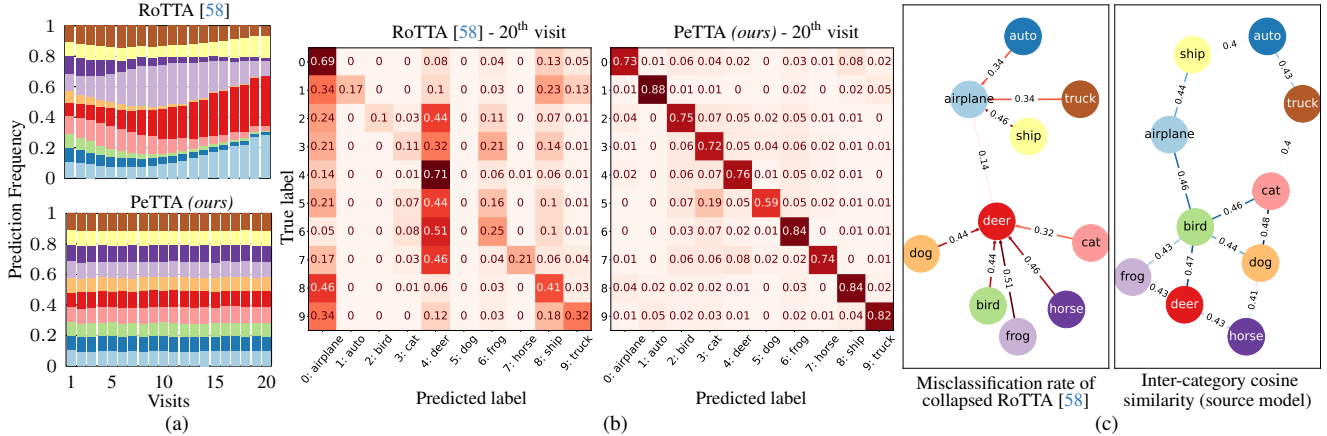


Figure 4. Episodic TTA (20 visits) on CIFAR→CIFAR10-C task. (a) Histogram of model predictions (labels are color-coded). PeTTA achieves a persisting performance while RoTTA [58] degrades. (b) Confusion matrix at the last visit, RoTTA [58] classifies all samples into a few categories (e.g., 0: *airplane*, 4: *deer*). (c) Force-directed graph showing (left) the most prone to misclassification pairs (arrows indicating the portion and pointing from the true to the misclassified category); (right) similar categories tend to be easily collapsed. Edges denote the average cosine similarity of feature vectors (source model), only the highest similar pairs are shown. Best viewed in color.

Table 3. Average (across 20 visits) error of multiple variations of PeTTA: without (w/o) regularization term $\mathcal{R}(\theta)$, fixed regularization coefficient λ ; adaptive coefficient λ_t , update rate α_t , and anchor loss \mathcal{L}_{AL} .

Method	CF-10-C	CF-100-C	DN	IN-C
Baseline w/o $\mathcal{R}(\theta)$	42.6	63.0	77.9	93.4
$\mathcal{R}(\theta)$ fixed $\lambda = 0.1\lambda_0$	43.3	65.0	80.0	92.5
$\mathcal{R}(\theta)$ fixed $\lambda = \lambda_0$	42.0	64.6	66.6	92.9
PeTTA - λ_t	27.1	55.0	59.7	92.7
PeTTA - $\lambda_t + \alpha_t$	23.9	41.4	44.5	75.7
PeTTA - $\lambda_t + \mathcal{L}_{AL}$	26.2	36.3	43.2	62.0
PeTTA - $\lambda_t + \alpha_t + \mathcal{L}_{AL}$	22.8	35.1	42.9	60.5

Table 4. Average (across 20 visits) error of PeTTA. PeTTA favors various choices of regularizers $\mathcal{R}(\theta)$: L2 and cosine similarity in conjunction with Fisher [27, 38] coefficient.

Method		CF-10-C	CF-100-C	DN	IN-C
$\mathcal{R}(\theta)$	Fisher				
L2	✗	23.0	35.6	43.1	70.8
	✓	22.7	36.0	43.9	70.0
Cosine	✗	22.8	35.1	42.9	60.5
	✓	22.6	35.9	43.3	63.8

\mathcal{L}_{AL} is insufficient to guide the adaptation. Thus, leveraging all elements secures the persistence of PeTTA (row 7).

Various Choices of Regularizers. The design of PeTTA is not coupled with any specific regularization term. Demonstrated in Tab. 4, PeTTA works well for the two common choices: L2 and cosine similarity. We also investigate the conjunction use of Fisher coefficient [27, 38] for weighting the model parameter importance. While the benefit (in terms of improving accuracy) varies across datasets, PeTTA

accommodates all choices, as the model collapse is not observed in any of the options.

7. Discussion and Conclusion

On a Potential Risk of TTA in Practice. We provide empirical and theoretical evidence on the risk of deploying continual TTA algorithms. Existing studies fail to detect this issue with *a single pass per test set*. The recurring TTA could be conveniently adopted as a *straightforward evaluation*, where its challenging test stream magnifies the error accumulation that a model might encounter in practice.

Limitations. PeTTA takes one step toward mitigating the gradual performance degradation of TTA. Nevertheless, a complete elimination of error accumulation cannot be guaranteed rigorously through regularization. Future research could delve deeper into expanding our efforts to develop an algorithm that achieves error accumulation-free by construction. Furthermore, as tackling the challenge of the temporally correlated testing stream is not the focus of PeTTA, using a small memory bank as in [15, 58] is necessary. It also assumes the features statistics from the source distribution are available (Appdx. D.3, D.4). These constraints potentially limit its scalability in real-world scenarios.

Conclusion. Towards trustworthy and reliable TTA applications, we rigorously study the *performance degradation problem of TTA*. The proposed *recurring TTA* setting highlights the limitations of modern TTA methods, which struggle to prevent the error accumulation when continuously adapting to demanding test streams. Theoretically inspecting a failure case of ϵ -*GMMC* paves the road for designing PeTTA- a simple yet efficient solution that continuously assesses the model divergence for harmonizing the TTA process, balancing adaptation, and collapse prevention.

Acknowledgement

This work was supported by the Jump ARCHES Endowment through the Health Care Engineering Systems Center, in part by the National Institute of Health (NIH) under Grant R01 AI139401, and in part by the Vingroup Innovation Foundation under Grant VINIF.2021.DA00128.

References

- [1] Kartik Ahuja, Ethan Caballero, Dinghuai Zhang, Jean-Christophe Gagnon-Audet, Yoshua Bengio, Ioannis Mitliakos, and Irina Rish. Invariance principle meets information bottleneck for out-of-distribution generalization. In *Advances in Neural Information Processing Systems*, 2021. 1
- [2] Rahaf Aljundi, Eugene Belilovsky, Tinne Tuytelaars, Laurent Charlin, Massimo Caccia, Min Lin, and Lucas Page-Caccia. Online continual learning with maximal interfered retrieval. In *Advances in Neural Information Processing Systems*, 2019. 2
- [3] Rahaf Aljundi, Min Lin, Baptiste Goujaud, and Yoshua Bengio. Gradient based sample selection for online continual learning. In *Advances in Neural Information Processing Systems*, 2019. 2
- [4] Amitav Banerjee, U. B. Chitnis, S. L. Jadhav, J. S. Bhawalkar, and S. Chaudhury. Hypothesis testing, type I and type II errors. *Industrial Psychiatry Journal*, 18(2):127–131, 2009. 4
- [5] Richard Bellman. *Dynamic Programming*. Princeton University Press, Princeton, NJ, USA, 1957. 5
- [6] Arno Blaas, Andrew Miller, Luca Zappella, Joern-Henrik Jacobsen, and Christina Heinze-Deml. Considerations for distribution shift robustness in health. In *ICLR 2023 Workshop on Trustworthy Machine Learning for Healthcare*, 2023. 1
- [7] Malik Boudiaf, Romain Mueller, Ismail Ben Ayed, and Luca Bertinetto. Parameter-free online test-time adaptation. In *2022 IEEE/CVF Conference on Computer Vision and Pattern Recognition (CVPR)*, pages 8334–8343, 2022. 2, 3, 6, 7, 20, 21
- [8] Dian Chen, Dequan Wang, Trevor Darrell, and Sayna Ebrahimi. Contrastive test-time adaptation. In *Proceedings of the IEEE International Conference on Computer Vision*, 2022. 1, 19, 26
- [9] Thomas M. Cover and Joy A. Thomas. *Elements of Information Theory (Wiley Series in Telecommunications and Signal Processing)*. Wiley-Interscience, USA, 2006. 5
- [10] Francesco Croce, Maksym Andriushchenko, Vikash Sehwag, Edoardo Debenedetti, Nicolas Flammarion, Mung Chiang, Prateek Mittal, and Matthias Hein. Robustbench: a standardized adversarial robustness benchmark. In *Thirty-fifth Conference on Neural Information Processing Systems Datasets and Benchmarks Track*, 2021. 6, 23, 26
- [11] Matthias De Lange, Rahaf Aljundi, Marc Masana, Sarah Parisot, Xu Jia, Ales Leonardis, Gregory Slabaugh, and Tinne Tuytelaars. A continual learning survey: Defying forgetting in classification tasks. *IEEE Transactions on Pattern Analysis and Machine Intelligence*, 44(7):3366–3385, 2022. 2
- [12] Mario Döbler, Robert A. Marsden, and Bin Yang. Robust mean teacher for continual and gradual test-time adaptation. In *Proceedings of the IEEE/CVF Conference on Computer Vision and Pattern Recognition (CVPR)*, pages 7704–7714, 2022. 1, 2, 3, 5, 6, 7, 19, 20, 21, 26, 27
- [13] Yaroslav Ganin and Victor Lempitsky. Unsupervised domain adaptation by backpropagation. In *Proceedings of the 32nd International Conference on Machine Learning*, pages 1180–1189, Lille, France, 2015. PMLR. 1, 6
- [14] Yaroslav Ganin, Evgeniya Ustinova, Hana Ajakan, Pascal Germain, Hugo Larochelle, François Laviolette, Mario Marchand, and Victor Lempitsky. *Domain-Adversarial Training of Neural Networks*, pages 189–209. Springer International Publishing, 2017. 1
- [15] Taesik Gong, Jongheon Jeong, Taewon Kim, Yewon Kim, Jinwoo Shin, and Sung-Ju Lee. NOTE: Robust continual test-time adaptation against temporal correlation. In *Advances in Neural Information Processing Systems*, 2022. 2, 3, 8, 16, 19
- [16] Yves Grandvalet and Yoshua Bengio. Semi-supervised learning by entropy minimization. In *Advances in Neural Information Processing Systems*, 2004. 3, 5
- [17] Kaiming He, Xiangyu Zhang, Shaoqing Ren, and Jian Sun. Deep residual learning for image recognition. *arXiv preprint arXiv:1512.03385*, 2015. 26
- [18] Kaiming He, Xiangyu Zhang, Shaoqing Ren, and Jian Sun. Delving deep into rectifiers: Surpassing human-level performance on ImageNet classification. In *Proceedings of the IEEE Conference on Computer Vision and Pattern Recognition (CVPR)*, pages 1026–1034, 2015. 1
- [19] Dan Hendrycks and Thomas Dietterich. Benchmarking neural network robustness to common corruptions and perturbations. *Proceedings of the International Conference on Learning Representations*, 2019. 1, 2, 6, 7, 21, 22, 23, 24, 25, 26, 27
- [20] Dan Hendrycks, Norman Mu, Ekin D. Cubuk, Barret Zoph, Justin Gilmer, and Balaji Lakshminarayanan. AugMix: A simple data processing method to improve robustness and uncertainty. *Proceedings of the International Conference on Learning Representations (ICLR)*, 2020. 26
- [21] Dan Hendrycks, Steven Basart, Norman Mu, Saurav Kadavath, Frank Wang, Evan Dorundo, Rahul Desai, Tyler Zhu, Samyak Parajuli, Mike Guo, Dawn Song, Jacob Steinhardt, and Justin Gilmer. The many faces of robustness: A critical analysis of out-of-distribution generalization. In *2021 IEEE/CVF International Conference on Computer Vision (ICCV)*, pages 8320–8329, 2021. 1
- [22] Junyuan Hong, Lingjuan Lyu, Jiayu Zhou, and Michael Spranger. MECTA: Memory-economic continual test-time model adaptation. In *The Eleventh International Conference on Learning Representations*, 2023. 2, 6, 7, 19, 20, 21
- [23] Fabian Isensee, Paul F. Jaeger, Simon A. A. Kohl, Jens Petersen, and Klaus H. Maier-Hein. nnU-Net: a self-configuring method for deep learning-based biomedical image segmentation. *Nature Methods*, 18(2):203–211, 2021. 1

- [24] Yusuke Iwasawa and Yutaka Matsuo. Test-time classifier adjustment module for model-agnostic domain generalization. In *Advances in Neural Information Processing Systems*, pages 2427–2440, 2021. 1
- [25] Michael N. Katehakis and Arthur F. Veinott. The multi-armed bandit problem: Decomposition and computation. *Mathematics Operations Research*, 12:262–268, 1987. 5
- [26] Diederik P. Kingma and Jimmy Ba. Adam: A method for stochastic optimization. In *3rd International Conference on Learning Representations, ICLR 2015, San Diego, CA, USA, May 7-9, 2015, Conference Track Proceedings*, 2015. 26
- [27] James Kirkpatrick, Razvan Pascanu, Neil Rabinowitz, Joel Veness, Guillaume Desjardins, Andrei A. Rusu, Kieran Milan, John Quan, Tiago Ramalho, Agnieszka Grabska-Barwinska, Demis Hassabis, Claudia Clopath, Dharshan Kumaran, and Raia Hadsell. Overcoming catastrophic forgetting in neural networks. *Proceedings of the National Academy of Sciences*, 114(13):3521–3526, 2017. 2, 5, 8
- [28] Dong-Hyun Lee. Pseudo-label : The simple and efficient semi-supervised learning method for deep neural networks. *ICML 2013 Workshop : Challenges in Representation Learning (WREPL)*, 2013. 3
- [29] Haoliang Li, Sinno Jialin Pan, Shiqi Wang, and Alex C. Kot. Domain generalization with adversarial feature learning. In *Proceedings of the IEEE Conference on Computer Vision and Pattern Recognition (CVPR)*, 2018. 1
- [30] Yanghao Li, Naiyan Wang, Jianping Shi, Jiaying Liu, and Xiaodi Hou. Revisiting batch normalization for practical domain adaptation. In *International Conference on Learning Representations Workshop*, 2017. 5
- [31] Zhizhong Li and Derek Hoiem. Learning without forgetting. *IEEE Transactions on Pattern Analysis and Machine Intelligence*, 40(12):2935–2947, 2018. 5, 20
- [32] Jian Liang, Dapeng Hu, and Jiashi Feng. Do we really need to access the source data? Source hypothesis transfer for unsupervised domain adaptation. In *International Conference on Machine Learning (ICML)*, pages 6028–6039, 2020. 2
- [33] Sen Lin, Peizhong Ju, Yingbin Liang, and Ness Shroff. Theory on forgetting and generalization of continual learning. In *Proceedings of the 40th International Conference on Machine Learning*, 2023. 2
- [34] TorchVision maintainers and contributors. Torchvision: Pytorch’s computer vision library. <https://github.com/pytorch/vision>, 2016. 6, 26
- [35] Robert A Marsden, Mario Döbler, and Bin Yang. Gradual test-time adaptation by self-training and style transfer. *arXiv preprint arXiv:2208.07736*, 2022. 2
- [36] Ben Mildenhall, Pratul P. Srinivasan, Matthew Tancik, Jonathan T. Barron, Ravi Ramamoorthi, and Ren Ng. NeRF: Representing scenes as neural radiance fields for view synthesis. In *Proceedings of the European Conference on Computer Vision (ECCV)*, 2020. 1
- [37] A. Tuan Nguyen, Thanh Nguyen-Tang, Ser-Nam Lim, and Philip Torr. TIPI: Test time adaptation with transformation invariance. In *Conference on Computer Vision and Pattern Recognition 2023*, 2023. 1, 2
- [38] Shuaicheng Niu, Jiaxiang Wu, Yifan Zhang, Yaofu Chen, Shijian Zheng, Peilin Zhao, and Mingkui Tan. Efficient test-time model adaptation without forgetting. In *The International Conference on Machine Learning*, 2022. 2, 4, 5, 6, 8, 16, 19
- [39] Shuaicheng Niu, Jiaxiang Wu, Yifan Zhang, Zhiqian Wen, Yaofu Chen, Peilin Zhao, and Mingkui Tan. Towards stable test-time adaptation in dynamic wild world. In *The Eleventh International Conference on Learning Representations*, 2023. 1, 2
- [40] K. R. Parthasarathy. *Introduction to Probability and Measure*. Hindustan Book Agency, Gurgaon, 2005. 15
- [41] Adam Paszke, Sam Gross, Francisco Massa, Adam Lerer, James Bradbury, Gregory Chanan, Trevor Killeen, Zeming Lin, Natalia Gimelshein, Luca Antiga, Alban Desmaison, Andreas Köpf, Edward Yang, Zach DeVito, Martin Raison, Alykhan Tejani, Sasank Chilamkurthy, Benoit Steiner, Lu Fang, Junjie Bai, and Soumith Chintala. Pytorch: An imperative style, high-performance deep learning library, 2019. 6
- [42] Xingchao Peng, Qinxun Bai, Xide Xia, Zijun Huang, Kate Saenko, and Bo Wang. Moment matching for multi-source domain adaptation. In *Proceedings of the IEEE International Conference on Computer Vision*, pages 1406–1415, 2019. 6, 21, 23, 25, 26, 27
- [43] Ori Press, Steffen Schneider, Matthias Kueimmerer, and Matthias Bethge. RDumb: A simple approach that questions our progress in continual test-time adaptation. In *Thirty-seventh Conference on Neural Information Processing Systems*, 2023. 2, 6, 7, 16, 20, 21, 23, 24
- [44] Joaquin Quionero-Candela, Masashi Sugiyama, Anton Schwaighofer, and Neil D. Lawrence. *Dataset Shift in Machine Learning*. The MIT Press, 2009. 1, 3
- [45] Alec Radford, Jong Wook Kim, Chris Hallacy, Aditya Ramesh, Gabriel Goh, Sandhini Agarwal, Girish Sastry, Amanda Askell, Pamela Mishkin, Jack Clark, Gretchen Krueger, and Ilya Sutskever. Learning transferable visual models from natural language supervision. In *Proceedings of the 38th International Conference on Machine Learning*, pages 8748–8763. PMLR, 2021. 1
- [46] Benjamin Recht, Rebecca Roelofs, Ludwig Schmidt, and Vaishal Shankar. Do ImageNet classifiers generalize to ImageNet? In *Proceedings of the 36th International Conference on Machine Learning*, pages 5389–5400. PMLR, 2019. 1
- [47] Moowoon Rhee and Tohyun Kim. *Exploration and Exploitation*, pages 543–546. Palgrave Macmillan UK, London, 2018. 5
- [48] Matthew Riemer, Ignacio Cases, Robert Ajemian, Miao Liu, Irina Rish, Yuhai Tu, , and Gerald Tesauro. Learning to learn without forgetting by maximizing transfer and minimizing interference. In *International Conference on Learning Representations*, 2019. 2
- [49] Tanin Sirimongkolkasem and Reza Drikvandi. On Regularisation Methods for Analysis of High Dimensional Data. *Annals of Data Science*, 6(4):737–763, 2019. 5
- [50] Yu Sun, Xiaolong Wang, Zhuang Liu, John Miller, Alexei Efros, and Moritz Hardt. Test-time training with self-supervision for generalization under distribution shifts. In

- Proceedings of the 37th International Conference on Machine Learning*, pages 9229–9248. PMLR, 2020. [1](#), [2](#)
- [51] Richard S. Sutton and Andrew G. Barto. *Reinforcement Learning: An Introduction*. MIT Press, Cambridge, MA, 2018. [5](#)
- [52] Antti Tarvainen and Harri Valpola. Mean teachers are better role models: Weight-averaged consistency targets improve semi-supervised deep learning results. In *Proceedings of the 31st International Conference on Neural Information Processing Systems*, page 1195–1204, 2017. [2](#), [3](#)
- [53] Daniel Vela, Andrew Sharp, Richard Zhang, Trang Nguyen, An Hoang, and Oleg S. Pinykh. Temporal quality degradation in AI models. *Scientific Reports*, 12(1):11654, 2022. [2](#)
- [54] Dequan Wang, Evan Shelhamer, Shaoteng Liu, Bruno Olshausen, and Trevor Darrell. Tent: Fully test-time adaptation by entropy minimization. In *International Conference on Learning Representations*, 2021. [1](#), [2](#), [3](#), [26](#)
- [55] Jindong Wang, Cuiling Lan, Chang Liu, Yidong Ouyang, and Tao Qin. Generalizing to unseen domains: A survey on domain generalization. In *Proceedings of the Thirtieth International Joint Conference on Artificial Intelligence, IJCAI-21*, pages 4627–4635. International Joint Conferences on Artificial Intelligence Organization, 2021. Survey Track. [1](#)
- [56] Qin Wang, Olga Fink, Luc Van Gool, and Dengxin Dai. Continual test-time domain adaptation. In *Proceedings of the IEEE/CVF Conference on Computer Vision and Pattern Recognition (CVPR)*, pages 7201–7211, 2022. [1](#), [2](#), [3](#), [5](#), [6](#), [7](#), [16](#), [19](#), [20](#), [21](#), [26](#)
- [57] Zachary Young and Robert Steele. Empirical evaluation of performance degradation of machine learning-based predictive models – a case study in healthcare information systems. *International Journal of Information Management Data Insights*, 2(1):100070, 2022. [2](#)
- [58] Longhui Yuan, Binhui Xie, and Shuang Li. Robust test-time adaptation in dynamic scenarios. In *Proceedings of the IEEE/CVF Conference on Computer Vision and Pattern Recognition*, pages 15922–15932, 2023. [1](#), [2](#), [3](#), [5](#), [6](#), [7](#), [8](#), [16](#), [17](#), [19](#), [20](#), [21](#), [24](#), [26](#), [27](#), [28](#)
- [59] Hao Zhao, Yuejiang Liu, Alexandre Alahi, and Tao Lin. On pitfalls of test-time adaptation. In *ICLR 2023 Workshop on Pitfalls of limited data and computation for Trustworthy ML*, 2023. [2](#), [5](#)

Persistent Test-time Adaptation in Recurring Testing Scenarios

Technical Appendices

Table of Contents

A Proof of Lemmas and Theorems	13
A.1 Proof of Lemma 1	13
A.2 Proof of Lemma 2.	14
A.3 Proof of Theorem 1 and Corollary 1.	15
B Further Justifications on Gaussian Mixture Model Classifier	16
C Further Justifications on the Recurring Testing Scenario	16
C.1. Recurring TTA Follows the Design of a Practical TTA Stream	16
C.2 Recurring TTA as a Diagnostic Tool	16
C.3. Recurring TTA with Random Orders	16
D Further Justifications on Persistent TTA (PeTTA)	18
D.1 Pseudo Code	18
D.2 Anchor Loss	18
D.3 The Use of the Memory Bank	19
D.4 Empirical Mean and Covariant Matrix of Feature Vectors on the Source Dataset	19
D.5 Novelty of PeTTA	20
E Additional Experimental Results of PeTTA	20
E.1. Performance of PeTTA Versus Compared Methods	20
E.2. An Inspection of PeTTA	21
E.3. Does Model Reset Help?	21
E.4. PeTTA with Continuously Changing Corruption (CCC) Setting	24
E.5. More Details on the Ablation Study	24
E.6. More Confusion Matrices in Recurring TTA Setting	26
F. Experimental Details	26
F.1. Computing Resources	26
F.2. Test-time Adaptation Methods	26
F.3. The Use of Existing Assets	27

A. Proof of Lemmas and Theorems

In this section, we prove the theoretical results regarding the ϵ -perturbed Gaussian Mixture Model Classifier (ϵ -GMMC) introduced in Section 4.2. We first briefly summarize the definition of model collapse and the static data stream assumption:

Definition 1 (Model Collapse). *A model is said to be collapsed from step $\tau \in \mathcal{T}, \tau < \infty$ if there exists a non-empty subset of categories $\tilde{\mathcal{Y}} \subset \mathcal{Y}$ such that $\Pr\{Y_t \in \tilde{\mathcal{Y}}\} > 0$ but the marginal $\Pr\{\hat{Y}_t \in \tilde{\mathcal{Y}}\}$ converges to zero in probability:*

$$\lim_{t \rightarrow \tau} \Pr\{\hat{Y}_t \in \tilde{\mathcal{Y}}\} = 0.$$

Assumption 1 (Static Data Stream). *The marginal distribution of the true label follows the same Bernoulli distribution $\text{Ber}(p_0)$: $p_{0,t} = p_0, (p_{1,t} = p_1 = 1 - p_0), \forall t \in \mathcal{T}$.*

Preliminary. Following the same set of notations introduced in the main text, recall that we denoted $p_{y,t} \triangleq \Pr\{Y_t = y\}$, $\hat{p}_{y,t} \triangleq \Pr\{\hat{Y}_t = y\}$ (marginal distribution of the true label Y_t and pseudo label \hat{Y}_t receiving label y , respectively) and $\epsilon_t = \Pr\{Y_t = 1 | \hat{Y}_t = 0\}$ (the false negative rate (FNR) of ϵ -GMMC). At testing step t , we obtain the following relations:

$$\mathbb{E}_{P_t} [X_t | \hat{Y}_t = 0] = (1 - \epsilon_t)\mu_0 + \epsilon_t\mu_1, \quad (9)$$

$$\mathbb{E}_{P_t} [X_t | \hat{Y}_t = 1] = \mu_1, \quad (10)$$

$$\text{Var}_{P_t} (X_t | \hat{Y}_t = 0) = (1 - \epsilon_t)\sigma_0^2 + \epsilon_t\sigma_1^2 + \epsilon_t(1 - \epsilon_t)(\mu_0 - \mu_1)^2, \quad (11)$$

$$\text{Var}_{P_t} (X_t | \hat{Y}_t = 1) = \sigma_1^2. \quad (12)$$

In addition, under Assumption 1, the marginal distribution $P_t(x)$ (also referred as *data distribution* in our setup) is:

$$P_t(x) = \mathcal{N}(x; p_0\mu_0 + p_1\mu_1, p_0\sigma_0^2 + p_1\sigma_1^2 + p_0p_1(\mu_0 - \mu_1)^2) \quad \forall t \in \mathcal{T}. \quad (13)$$

A.1. Proof of Lemma 1

Lemma 1 (Increasing FNR). *Under Assumption 1, a binary ϵ -GMMC would collapsed (Def. 1) with $\lim_{t \rightarrow \tau} \hat{p}_{1,t} = 0$ (or $\lim_{t \rightarrow \tau} \hat{p}_{0,t} = 1$, equivalently) if and only if $\lim_{t \rightarrow \tau} \epsilon_t = p_1$.*

Proof. Under Assumption 1, we have $\mathbb{E}_{P_t} [X_t] = p_0\mu_0 + (1 - p_0)\mu_1$. Also note that:

$$\begin{aligned} \mathbb{E}_{P_t} [X_t] &= \mathbb{E}_{P_t} [\mathbb{E}_{P_t} [X_t | \hat{Y}_t]] \\ &= \mathbb{E}_{P_t} [X_t | \hat{Y}_t = 0] \hat{p}_{0,t} + \mathbb{E}_{P_t} [X_t | \hat{Y}_t = 1] \hat{p}_{1,t} \\ &= [(1 - \epsilon_t)\mu_0 + \epsilon_t\mu_1] \hat{p}_{0,t} + \mu_1(1 - \hat{p}_{0,t}) \\ &= [(1 - \epsilon_t)\hat{p}_{0,t}] \mu_0 + [1 - \hat{p}_{0,t}(1 - \epsilon_t)] \mu_1 \\ &= p_0\mu_0 + (1 - p_0)\mu_1, \end{aligned} \quad (14)$$

where the second equality follows Eqs. 9-10. Therefore:

$$\hat{p}_{0,t} = \frac{p_0}{1 - \epsilon_t}. \quad (15)$$

Eq. 15 shows positive correlation between $\hat{p}_{0,t}$ and ϵ_t . Given $\lim_{t \rightarrow \tau} \epsilon_t = p_1$, taking the limit introduces:

$$\lim_{t \rightarrow \tau} \hat{p}_{0,t} = \lim_{t \rightarrow \tau} \frac{p_0}{1 - \epsilon_t} = \frac{p_0}{1 - p_1} = 1.$$

Similarly, having $\lim_{t \rightarrow \tau} \hat{p}_{0,t} = 1$, the false negative rate ϵ_t when $t \rightarrow \tau$ is:

$$\lim_{t \rightarrow \tau} \epsilon_t = 1 - p_0 = p_1.$$

Since $\hat{p}_{0,t} + \hat{p}_{1,t} = 1$, $\lim_{t \rightarrow \tau} \hat{p}_{1,t} = 0$, equivalently. Towards the collapsing point, the model tends to predict a single label (class 0 in the current setup). In addition, the FNR of the model ϵ_t also raises correspondingly. \square

A.2. Proof of Lemma 2.

Lemma 2 (ϵ -GMMC After Collapsing). For a binary ϵ -GMMC model, with Assumption 1, if $\lim_{t \rightarrow \tau} \hat{p}_{1,t} = 0$ (collapsing), the cluster 0 in GMMC converges in distribution to a single-cluster GMMC with parameters:

$$\mathcal{N}(\hat{\mu}_{0,t}, \hat{\sigma}_{0,t}^2) \xrightarrow{d} \mathcal{N}(p_0\mu_0 + p_1\mu_1, p_0\sigma_0^2 + p_1\sigma_1^2 + p_0p_1(\mu_0 - \mu_1)^2).$$

Proof. From Eqs. 9-10, under the increasing type II collapse of ϵ -GMMC setting, the perturbation does not affect the approximation of μ_1 . Meanwhile, when ϵ_t increases, one can expect that $\hat{\mu}_{0,t}$ moves further away from μ_0 toward μ_1 . Frist, the mean teacher model of GMMC (Eq. 4, main text) gives:

$$\begin{aligned} \mathbb{E}_{P_t} [\hat{\mu}_{0,t} | \hat{Y}_t = 1] &= \mathbb{E}_{P_{t-1}} [\hat{\mu}_{0,t-1}], \\ \mathbb{E}_{P_t} [\hat{\mu}_{0,t} | \hat{Y}_t = 0] &= (1 - \alpha)\mathbb{E}_{P_{t-1}} [\hat{\mu}_{0,t-1} | \hat{Y}_t = 0] + \alpha\mathbb{E}_{P_t} [X_t | \hat{Y}_t = 0] \\ &= (1 - \alpha)\mathbb{E}_{P_{t-1}} [\hat{\mu}_{0,t-1}] + \alpha \left(\mathbb{E}_{P_t} [X_t | \hat{Y}_t = 0] \right), \\ \mathbb{E}_{P_t} [\hat{\mu}_{1,t} | \hat{Y}_t = 1] &= (1 - \alpha)\mathbb{E}_{P_{t-1}} [\hat{\mu}_{1,t-1} | \hat{Y}_t = 1] + \alpha\mathbb{E}_{P_t} [X_t | \hat{Y}_t = 1] \\ &= (1 - \alpha)\mathbb{E}_{P_{t-1}} [\hat{\mu}_{1,t-1}] + \alpha \left(\mathbb{E}_{P_t} [X_t | \hat{Y}_t = 1] \right), \\ \mathbb{E}_{P_t} [\hat{\mu}_{1,t} | \hat{Y}_t = 0] &= \mathbb{E}_{P_{t-1}} [\hat{\mu}_{1,t-1}]. \end{aligned}$$

By defining $u_{y,t} = \mathbb{E}_{P_t} [\hat{\mu}_{y,t}]$, we obtain the following recurrence relation between $u_{0,t}$ and $u_{0,t-1}$:

$$\begin{aligned} u_{0,t} &= \mathbb{E}_{P_t} [\hat{\mu}_{0,t} | \hat{Y}_t = 0] \hat{p}_{0,t} + \mathbb{E}_{P_t} [\hat{\mu}_{0,t} | \hat{Y}_t = 1] \hat{p}_{1,t} \\ &= \left((1 - \alpha)u_{0,t-1} + \alpha\mathbb{E}_{P_t} [X_t | \hat{Y}_t = 0] \right) \hat{p}_{0,t} + u_{0,t-1} \hat{p}_{1,t} \\ &= [(1 - \alpha)\hat{p}_{0,t} + \hat{p}_{1,t}] u_{0,t-1} + \alpha\hat{p}_{0,t} \mathbb{E}_{P_t} [X_t | \hat{Y}_t = 0] \\ &= (1 - \alpha\hat{p}_{0,t})u_{0,t-1} + \alpha\hat{p}_{0,t} \mathbb{E}_{P_t} [X_t | \hat{Y}_t = 0] \\ &= (1 - \alpha\hat{p}_{0,t})u_{0,t-1} + \alpha\hat{p}_{0,t} [(1 - \epsilon_t)\mu_0 + \epsilon_t\mu_1]. \end{aligned} \tag{16}$$

Given $\lim_{t \rightarrow \tau} \hat{p}_{0,t} = 1$, it follows that $\lim_{t \rightarrow \tau} \epsilon_{0,t} = p_1$ by Lemma 1. From this point:

$$u_{0,t} = (1 - \alpha)u_{0,t-1} + \alpha(p_0\mu_0 + p_1\mu_1) \quad \forall t > \tau.$$

Taking the limit $t \rightarrow \infty$:

$$\begin{aligned} \lim_{t \rightarrow \infty} u_{0,t} &= \lim_{t \rightarrow \infty} (1 - \alpha)u_{0,t-1} + \alpha(p_0\mu_0 + p_1\mu_1) \\ &= \lim_{t \rightarrow \infty} (1 - \alpha)^t \hat{\mu}_{0,0} + \alpha \sum_{i=1}^t (1 - \alpha)^{i-1} (p_0\mu_0 + p_1\mu_1) \\ &= \lim_{t \rightarrow \infty} (1 - \alpha)^t \hat{\mu}_{0,0} + (1 - (1 - \alpha)^t)(p_0\mu_0 + p_1\mu_1) \\ &= p_0\mu_0 + p_1\mu_1. \end{aligned}$$

The second equation is obtained by solving the recurrence relation. When $\lim_{t \rightarrow \tau} \hat{p}_{0,t} = 1$, $\{\hat{\mu}_{y,t}\}_{y \in \{0,1\}}$ becomes a deterministic values. Hence, giving $u_{y,t} = \mathbb{E}_{P_t} [\hat{\mu}_{y,t}] = \hat{\mu}_{y,t} (\forall t > \tau)$ and

$$\lim_{t \rightarrow \infty} \hat{\mu}_{0,t} = \lim_{t \rightarrow \infty} u_{0,t} = p_0\mu_0 + p_1\mu_1. \tag{17}$$

Repeating the steps above with Eqs. 11-12 in place of Eqs. 9-10, we obtain a similar result for $\sigma_{0,t}^2$:

$$\lim_{t \rightarrow \infty} \hat{\sigma}_{0,t}^2 = p_0 \sigma_0^2 + p_1 \sigma_1^2 + p_0 p_1 (\mu_0 - \mu_1)^2. \quad (18)$$

By Lévy's continuity theorem (p. 302, [40]), from Eqs. 17-18, when $t \rightarrow \infty$, the estimated distribution of the first cluster $\mathcal{N}(x; \hat{\mu}_{0,t}, \hat{\sigma}_{0,t}^2)$ converges to the whole data distribution $P_t(x)$ (Eq. 13) when collapsing. \square

A.3. Proof of Theorem 1 and Corollary 1.

Theorem 1 (Convergence of ϵ -GMMC). For a binary ϵ -GMMC model, with Assumption 1, let the distance from $\hat{\mu}_{0,t}$ toward μ_1 is $d_t^{0 \rightarrow 1} = |\mathbb{E}_{P_t}[\hat{\mu}_{0,t}] - \mu_1|$, then:

$$d_t^{0 \rightarrow 1} - d_{t-1}^{0 \rightarrow 1} \leq \alpha \cdot p_0 \cdot \left(|\mu_0 - \mu_1| - \frac{d_{t-1}^{0 \rightarrow 1}}{1 - \epsilon_t} \right).$$

Proof. Substituting Eq. 15 into $\hat{p}_{0,t}$ of Eq. 16 gives:

$$u_{0,t} = \left(1 - \frac{\alpha p_0}{1 - \epsilon_t} \right) u_{0,t-1} + \frac{\alpha p_0}{1 - \epsilon_t} [(1 - \epsilon_t) \mu_0 + \epsilon_t \mu_1].$$

Hence, we have the distance from $u_{0,t}$ toward μ_1 :

$$\begin{aligned} |u_{0,t} - \mu_1| &= \left| \left(1 - \frac{\alpha p_0}{1 - \epsilon_t} \right) u_{0,t-1} + \alpha p_0 \mu_0 + \frac{\alpha p_0 \epsilon_t \mu_1}{1 - \epsilon_t} - \mu_1 \right| \\ &= \left| \left(1 - \frac{\alpha p_0}{1 - \epsilon_t} \right) (u_{0,t-1} - \mu_1) + \alpha p_0 \mu_0 + \frac{\alpha p_0 \epsilon_t \mu_1}{1 - \epsilon_t} - \frac{\alpha p_0 \mu_1}{1 - \epsilon_t} \right| \\ &= \left| \left(1 - \frac{\alpha p_0}{1 - \epsilon_t} \right) (u_{0,t-1} - \mu_1) + \alpha p_0 \mu_0 - \frac{\alpha p_0 \mu_1 (1 - \epsilon_t)}{1 - \epsilon_t} \right| \\ &= \left| \left(1 - \frac{\alpha p_0}{1 - \epsilon_t} \right) (u_{0,t-1} - \mu_1) + \alpha p_0 (\mu_0 - \mu_1) \right| \\ &\leq \left(1 - \frac{\alpha p_0}{1 - \epsilon_t} \right) |u_{0,t-1} - \mu_1| + \alpha p_0 |\mu_0 - \mu_1|. \end{aligned}$$

The last inequality holds due to the triangle inequality. Equivalently,

$$|u_{0,t} - \mu_1| - |u_{0,t-1} - \mu_1| \leq \alpha \cdot p_0 \cdot \left(|\mu_0 - \mu_1| - \frac{|u_{0,t-1} - \mu_1|}{1 - \epsilon_t} \right).$$

Let $d_t^{0 \rightarrow 1} = |\mathbb{E}_{P_t}[\hat{\mu}_{0,t}] - \mu_1|$, we conclude that:

$$d_t^{0 \rightarrow 1} - d_{t-1}^{0 \rightarrow 1} \leq \alpha \cdot p_0 \cdot \left(|\mu_0 - \mu_1| - \frac{d_{t-1}^{0 \rightarrow 1}}{1 - \epsilon_t} \right).$$

\square

Corollary 1 (A Condition for ϵ -GMMC Collapse). With fixed $p_0, \alpha, \mu_0, \mu_1$, ϵ -GMMC is collapsed if there exists a sequence of $\{\epsilon_t\}_{\tau - \Delta_\tau}^\tau$ ($\tau \geq \Delta_\tau > 0$) such that:

$$p_1 \geq \epsilon_t > 1 - \frac{d_{t-1}^{0 \rightarrow 1}}{|\mu_0 - \mu_1|}, \quad t \in [\tau - \Delta_\tau, \tau].$$

Proof. Initialized at μ_0 , ϵ -GMMC is collapsing when $\hat{\mu}_{0,t}$ converges to the mid-point $p_0 \mu_0 + p_1 \mu_1$ (Lemma 2), i.e., moving closer to μ_1 . From Thm. 1, the distance towards μ_1 $d_t^{0 \rightarrow 1} < d_{t-1}^{0 \rightarrow 1}$ if

$$|\mu_0 - \mu_1| - \frac{|u_{0,t-1} - \mu_1|}{1 - \epsilon_t} < 0 \Leftrightarrow |\mu_0 - \mu_1| < \frac{|u_{0,t-1} - \mu_1|}{1 - \epsilon_t} \Leftrightarrow \epsilon_t > 1 - \frac{|u_{0,t-1} - \mu_1|}{|\mu_0 - \mu_1|}.$$

When there exists this sequence $\{\epsilon_t\}_{\tau - \Delta_\tau}^\tau$ ($\tau \geq \Delta_\tau > 0$) it follows that $d_t^{0 \rightarrow 1} < d_{t-1}^{0 \rightarrow 1}$ and $\epsilon_t > \epsilon_{t-1}$ is guaranteed $\forall t \in [\tau - \Delta_\tau, \tau]$. Hence, $\lim_{t \rightarrow \tau} \epsilon_t = p_1$ (model collapsed, by Lemma 1). \square

B. Further Justifications on Gaussian Mixture Model Classifier

One may notice that in ϵ -GMMC (Sec. 4.2), the classifier is defined $f_t(x) = \operatorname{argmax}_{y \in \mathcal{Y}} \Pr(x|y; \theta_t)$ (maximum likelihood estimation) while in general, $f_t(x) = \operatorname{argmax}_{y \in \mathcal{Y}} \Pr(y|x; \theta_t)$ (maximum a posterior estimation), parameterized by a neural network. In this case, since the *equal prior* (i.e., $\Pr(y; \theta_t) = \Pr(y'; \theta_t), \forall y, y' \in \mathcal{C}$) is enforced in ϵ -GMMC, the two definitions are *equivalent*.

Proof. Having:

$$\begin{aligned} \operatorname{argmax}_{y \in \mathcal{Y}} \Pr(y|x; \theta_t) &= \operatorname{argmax}_{y \in \mathcal{Y}} \frac{\Pr(x|y; \theta_t) \Pr(y; \theta_t)}{\sum_{y' \in \mathcal{Y}} \Pr(x|y'; \theta_t) \Pr(y'; \theta_t)} \\ &= \operatorname{argmax}_{y \in \mathcal{Y}} \Pr(x|y; \theta_t). \end{aligned}$$

We conclude that the two definitions are equivalent. In fact, it is well-known that maximum likelihood estimation is a special case of maximum a posterior estimation when the prior is uniform. \square

C. Further Justifications on the Recurring Testing Scenario

C.1. Recurring TTA Follows the Design of a Practical TTA Stream

Note that in recurring TTA, besides the recurrence of environments (or corruptions) as in [38, 56], the distribution of class labels is also temporally correlated (non-i.i.d.) as suggested by [15, 58] to reflect the practical testing stream better. In short, recurring TTA is formed by recurring the environments of *practical TTA* scenario introduced in [58] multiple times (readers are encouraged to visit the original paper for additional motivations on this scenario).

C.2. Recurring TTA as a Diagnostic Tool

Noticeably, CoTTA [56] also performed 10-round repetition across multiple domain shifts to simulate a lifelong TTA testing stream just like our recurring TTA. However, the key difference is CoTTA assumes the distribution of class labels is i.i.d., which does not hold in many real-life testing scenarios as argued in [15, 58]. Our recurring TTA lifts this assumption and allows temporally correlated (non-i.i.d.) label distribution (more challenging, more practical). This extension allows *recurring TTA* to spot the risk of model collapse on CoTTA [56] and other methods. The *over-simplicity* of the repeating scheme in CoTTA for spotting performance degradation is also suggested in [43]. Clearly, it seems not to be a problem at first glance in Tab. 5 of [56] (CoTTA’s 10-round repetition), but in fact, the risk in CoTTA remains, as explored in our scenario and also on CCC [43].

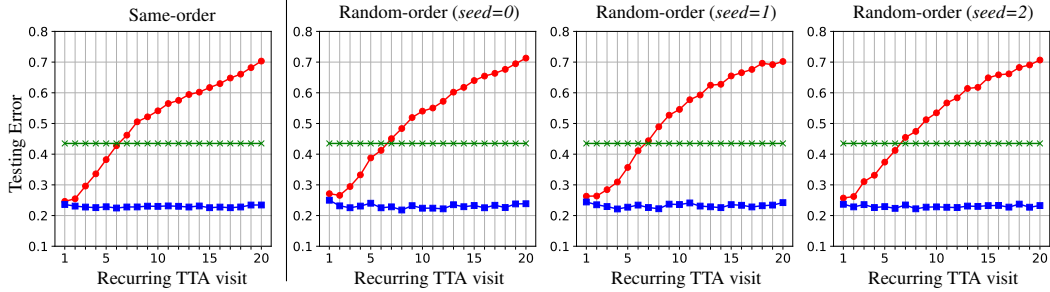
The construction of our recurring TTA is notably simple - a technical effort to extend the testing stream. However, this simplicity is on purpose, *servicing as a diagnostic tool for lifelong continual TTA*. Counterintuitively, our experiments on four different tasks with the latest methods verify that even if the model is exposed to the same environment (*the most basic case*), their adaptability and performance are still consistently reduced (demonstrated visually in Fig. 1, quantitatively in Sec. 6.3).

We believe that the extensive testing stream by recurrence in our setup is a *simple yet sufficient scenario* to demonstrate the vulnerability of existing continual TTA methods when facing the issue of model collapse (see Appdx. E.4 for comparison with CCC [43], a notably *more complicated scenario* than our recurring TTA). Indeed, recurring shifts are sufficient to show this failure mode and any lifelong TTA method should necessarily be able to handle recurring conditions.

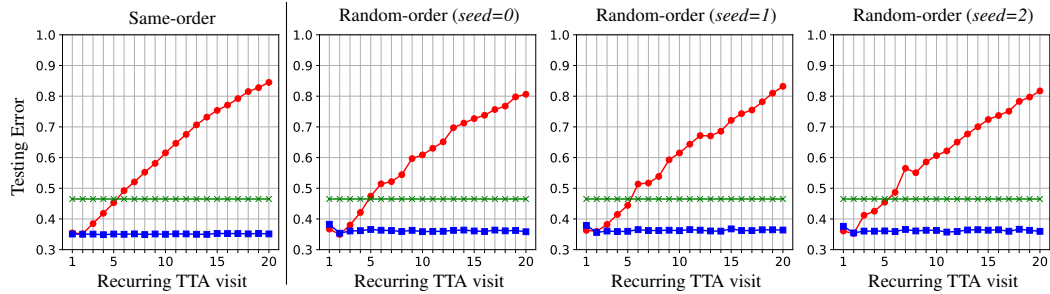
C.3. Recurring TTA with Random Orders

Recall that in Sec. 4.1, *recurring TTA* is constructed by repeating *the same* sequence of D distributions K times. For example, a sequence with $K = 2$ could be $\mathcal{P}_1 \rightarrow \mathcal{P}_2 \rightarrow \dots \rightarrow \mathcal{P}_D \rightarrow \mathcal{P}_1 \rightarrow \mathcal{P}_2 \rightarrow \dots \rightarrow \mathcal{P}_D$. For simplicity and consistency that promote reproducibility, the *same order of image corruptions* (following [58]) is used for all recurrences. This section presents supplementary experimental findings indicating that *the order of image corruptions* within each recurrence, indeed, *does not affect* the demonstration of TTA model collapse and the performance of our PeTTA.

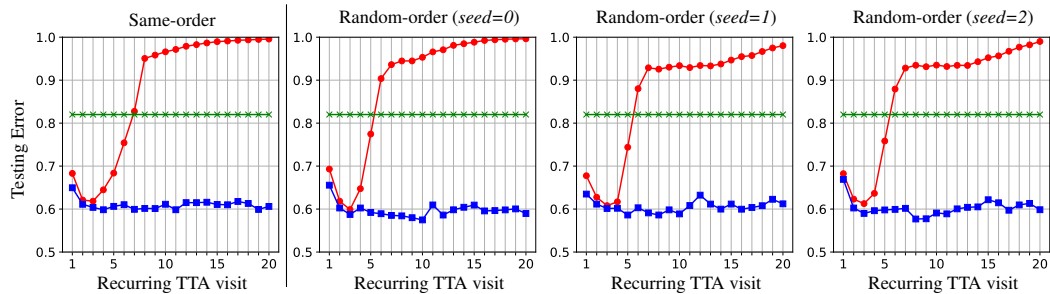
Experiment Setup. We refer to the setting *same-order* as using one order of image corruptions in [58] for all recurrences (specifically, on CIFAR-10/100-C and ImageNet-C: *motion* \rightarrow *snow* \rightarrow *fog* \rightarrow *shot* \rightarrow *defocus* \rightarrow *contrast* \rightarrow *zoom* \rightarrow *brightness* \rightarrow *frost* \rightarrow *elastic* \rightarrow *glass* \rightarrow *gaussian* \rightarrow *pixelated* \rightarrow *jpeg* \rightarrow *impulse*). Conversely, in *random-order*, the order of image corruptions is randomly shuffled at the beginning of each recurrence. Hence, the corruption orders across K recurrences are now entirely different. We redo the experiment of the second setting three times (with different random seeds = 0, 1, 2). Nevertheless, different TTA methods are ensured to be evaluated on the same testing stream, since it is fixed after



(a) CIFAR-10 \rightarrow CIFAR-10-C task.



(b) CIFAR-100 \rightarrow CIFAR-100-C task.



(c) ImageNet \rightarrow ImageNet-C task.

Figure 5. Recurring TTA with different order of corruptions. This figure plots the testing error of two TTA approaches: **RoTTA** \bullet - [58], and **PeTTA** \blacksquare - (*ours*), and **source model** \times - as a reference performance under our recurring TTA (with 20 visits) across three TTA tasks. On the *same-order* experiments (column 1), the same order of image corruptions is applied for all 20 visits. Meanwhile, in *random-order*, this order is reshuffled at the beginning of each visit (columns 2-4). Random-order experiments are redone three times with different random seeds. Here, we empirically validate that using the same order of domain shifts (image corruptions) in our recurring TTA is sufficient to showcase the model collapse and evaluate the persistence of our PeTTA. Best viewed in color.

generation. Without updating its parameters, the performance of the *source model* is trivially independent of the order of corruptions.

Experimental Result. The experimental results are visualized in Fig. 5. The first column plots the experiments under the *same-order*, while the remaining three columns plot the experiments in the *random-order* setting, with varying random seeds. Note that the message conveyed by each sub-figure entirely matches that of Fig. 1-right.

Discussions. Clearly, a similar collapsing pattern is observed in all three TTA tasks, with three combinations of 20 image corruption orders. This pattern also matches the easiest setting using the *same order* of image corruptions we promoted in *recurring TTA*.

Algorithm 1 Persistent TTA (PeTTA)

Input: Classification model f_t and its deep feature extractor ϕ_{θ_t} , both parameterized by $\theta_t \in \Theta$. Testing stream $\{X_t\}_{t=0}^T$, initial model parameter (θ_0), initial update rate (α_0), regularization term coefficient (λ_0), empirical mean ($\{\mu_0^y\}_{y \in \mathcal{Y}}$) and covariant matrix ($\{\Sigma_0^y\}_{y \in \mathcal{Y}}$) of feature vectors in the training set, $\hat{\mu}_t^y$ EMA update rate (ν).

```
1  $\hat{\mu}_0^y \leftarrow \mu_0^y, \forall y \in \mathcal{Y}$ ; // Initialization
2 for  $t \in [1, \dots, T]$  do
3    $\hat{Y}_t \leftarrow f_{t-1}(X_t)$ ; // Obtaining pseudo-labels for all samples in  $X_t$ 
4   // Persistent TTA (PeTTA)
5    $\hat{\mathcal{Y}}_t \leftarrow \{\hat{Y}_t^{(i)} | i = 1, \dots, N_t\}$ ; // Set of (unique) pseudo-labels in  $X_t$ 
6    $\bar{\gamma}_t \leftarrow 0$ ;
7   for  $y \in \hat{\mathcal{Y}}_t$  do
8      $\gamma_t^y \leftarrow 1 - \exp\left(-(\hat{\mu}_t^y - \mu_0^y)^T (\Sigma_0^y)^{-1} (\hat{\mu}_t^y - \mu_0^y)\right)$ ; // Divergence sensing term on category  $y$ 
9      $\bar{\gamma}_t \leftarrow \bar{\gamma}_t + \frac{\gamma_t^y}{|\hat{\mathcal{Y}}_t|}$ ; // Average divergence sensing term for step  $t$ 
10     $\hat{\mu}_t^y \leftarrow (1 - \nu)\hat{\mu}_{t-1}^y + \nu\phi_{\theta_{t-1}}(X_t | \hat{Y}_t = y)$ ; // EMA update of  $\hat{\mu}_t^y$  for samples with  $\hat{Y}_t = y$ 
11  end
12   $\lambda_t \leftarrow \bar{\gamma}_t \cdot \lambda_0$ ; // Computing adaptive regularization term coefficient
13   $\alpha_t \leftarrow (1 - \bar{\gamma}_t) \cdot \alpha_0$ ; // Computing adaptive update rate
14  // Regular Mean-teacher Update
15   $\theta'_t \leftarrow \text{Optim}_{\theta' \in \Theta} \mathbb{E}_{P_t} [\mathcal{L}_{\text{CLS}}(\hat{Y}_t, X_t; \theta') + \mathcal{L}_{\text{AL}}(X_t; \theta')] + \lambda_t \mathcal{R}(\theta')$ ; // Student model update
16   $\theta_t \leftarrow (1 - \alpha_t)\theta_{t-1} + \alpha_t\theta'_t$ ; // Teacher model update
17  // Final prediction
18  yield  $f_t(X_t)$ ; // Returning the final inference with updated model  $f_t$ 
19 end
```

D. Further Justifications on Persistent TTA (PeTTA)

D.1. Pseudo Code

We summarize the key steps of our proposed PeTTA in Alg. 1, with the key part (lines 4-13) [highlighted in blue](#). Our approach fits well in the general workflow of a TTA algorithm, *enhancing the regular mean-teacher update step*. Appdx. D.5 elaborates more on our contributions in PeTTA, distinguishing them from other components proposed in previous work. The notations and definitions of all components follow the main text (described in detail in Sec. 5). On line 8 of Alg. 1, as a shorthand notation, $\phi_{\theta_{t-1}}(X_t | \hat{Y}_t = y)$ denotes the empirical mean of all feature vectors of $X_t^{(i)}$ (extracted by $\phi_{\theta_{t-1}}(X_t^{(i)})$) if $\hat{Y}_t^{(i)} = y, i = 1, \dots, N_t$ in the current testing batch.

D.2. Anchor Loss

KL Divergence Minimization-based Interpretation of Anchor Loss. In Sec. 5, we claimed that minimizing the anchor loss \mathcal{L}_{AL} is equivalent to minimizing the relative entropy (or KL divergence) between the output probability of two models parameterized by θ_0 and θ .

Proof. Having:

$$\begin{aligned} D_{KL}(\Pr(y|X_t; \theta_0) || \Pr(y|X_t; \theta)) &= \sum_{y \in \mathcal{Y}} \Pr(y|X_t; \theta_0) \log \frac{\Pr(y|X_t; \theta_0)}{\Pr(y|X_t; \theta)} \\ &= \underbrace{- \sum_{y \in \mathcal{Y}} \Pr(y|X_t; \theta_0) \log \Pr(y|X_t; \theta)}_{\mathcal{L}_{\text{AL}}(X_t; \theta)} - \underbrace{H(\Pr(y|X_t; \theta_0))}_{\text{constant}}. \end{aligned}$$

Hence,

$$\operatorname{argmin}_{\theta \in \Theta} \mathcal{L}_{\text{AL}}(X_t; \theta) = \operatorname{argmin}_{\theta \in \Theta} D_{KL}(\Pr(y|X_t; \theta_0) || \Pr(y|X_t; \theta)).$$

□

Intuitively, a desirable TTA solution should be able to adapt to novel testing distributions on the one hand, but it should *not* significantly diverge from the initial model. \mathcal{L}_{AL} fits this purpose, constraining the KL divergence between two models at each step.

Connections between Anchor Loss and Regularizer Term. While supporting the same objective (collapse prevention by avoiding the model significantly diverging from the source model), the major difference between Anchor loss (\mathcal{L}_{AL}) and the Regularizer term ($\mathcal{R}(\theta)$) is that the anchor loss operates on the probability space of model prediction while the regularizer term works on the model parameter spaces. Tab. 3 (lines 1 and 5) summarizes the ablation study when each of them is eliminated. We see the role of the regularization term is crucial for avoiding model collapse, while the anchor loss guides the adaptation under the drastic domain shift. Nevertheless, fully utilizing all components is suggested for maintaining TTA persistence.

D.3. The Use of the Memory Bank

The size of Memory Bank. The size of the memory bank in PeTTA is *relatively small, equal to the size of one mini-batch for update* (64 images, specifically).

The Use of the Memory Bank in PeTTA is Fair with Respect To the Compared Methods. Our directly comparable method - RoTTA [58] also takes this advantage (referred to as category-balanced sampling, Sec. 3.2 of [58]). Hence, the comparison between PeTTA and RoTTA *is fair* in terms of additional memory usage. Noteworthy, the use of a memory bank is a *common practice* in TTA literature (e.g., [8, 15, 58]), especially in situations where the class labels are temporally correlated or non-i.i.d. distributed (as we briefly summarized in Appdx. 2 - Related Work section). CoTTA [56], EATA [38] and MECTA [22] (compared method) assume labels are i.i.d. distributed. Hence, a memory bank is unnecessary, but their performance under temporally correlated label distribution has dropped significantly as a trade-off. The RMT [12] (compared method) does not require a memory bank but it needs to cache a portion of the source training set for replaying (Sec. 3.3 in [12]) which even requires *more* resources than the memory bank.

Eliminating the Need for a Memory Bank. As addressing the challenge of temporally correlated label distribution on the testing stream is not the focus of PeTTA, we have conveniently adopted the use of the memory bank proposed in [58]. Since this small additional memory requirement is not universally applied in every real-world scenario, we believe that this is a reasonable assumption, and commonly adopted in TTA practices. Nevertheless, exploring alternative ways for reducing the memory size (e.g., storing the embedded features instead of the original image) would be an interesting future direction.

D.4. Empirical Mean and Covariant Matrix of Feature Vectors on the Source Dataset

Two Ways of Computing μ_0^y and Σ_0^y in Practice. One may notice that in PeTTA, computing γ_t^y requires the *pre-computed empirical mean (μ_0^y) and covariance (Σ_0^y) of the source dataset*. This requirement may not be met in real-world situations where the source data is unavailable. In practice, the empirical mean and covariance matrix computed on the source distribution can be provided in the following two ways:

1. Most ideally, these values are computed directly by inference on the entire training set once the model is fully trained. They will be provided alongside the source-distribution pre-trained model as a pair for running TTA.
2. With only the source pre-trained model available, assume we can sample a set of unlabeled data from the source distribution. The (pseudo) labels for them are obtained by inferring from the source model. Since the source model is well-performed in this case, using pseudo is approximately as good as the true label.

Accessing the Source Distribution Assumption in TTA. In fact, the second way is typically assumed to be possible in previous TTA methods such as EATA [38], and MECTA [22] (a compared method) to estimate a Fisher matrix (for anti-forgetting regularization purposes). Our work - PeTTA *follows the same second setup* as the previous approaches mentioned above. A variation of RMT [12] (a compared method) approach even requires having the fully labeled source data available at test-time for source replaying (Sec. 3.3 of [12]). This variation is used for comparison in our experiments.

We believe that having the empirical mean and covariant matrix pre-computed on a portion of the source distribution in PeTTA *is a reasonable assumption*. Even in the ideal way, revealing the statistics might not severely violate the risk of data privacy leakage or require notable additional computing resources.

Number of Samples Needed for Computation. To elaborate more on the feasibility of setting (2) mentioned above, we perform a small additional experiment on the performance of PeTTA while varying the number of samples used for computing the empirical mean and covariant matrix on the source distribution. In this setting, we use the test set of CIFAR-10, CIFAR-100, DomainNet validation set of ImageNet (original images, without corruption, or the *real* domain test set of DomainNet), representing samples from the source distribution. The total number of images is 10,000 in CIFAR-10/A00, 50,000 in ImageNet, and 69,622 in DomainNet. We randomly sample 25%, 50%, 75%, and 100% of the images in this set to run PeTTA for 20 rounds of recurring. The result is provided in Tab. 5 below.

Table 5. Average classification error of PeTTA (across 20 visits) with varying sizes of source samples used for computing feature empirical mean (μ_0^y) and covariant matrix (Σ_0^y).

TTA Task	25%	50%	75%	100%
CIFAR-10 \rightarrow CIFAR-10-C	22.96	22.99	23.03	22.75
CIFAR-100 \rightarrow CIFAR-100-C	35.01	35.11	35.09	35.15
DomainNet: <i>real</i> \rightarrow <i>clip</i> \rightarrow <i>paint</i> \rightarrow <i>sketch</i>	43.18	43.12	43.15	42.89
ImageNet \rightarrow ImageNet-C	61.37	59.68	61.05	60.46

The default choice of PeTTA is using 100% samples of the validation set of the source dataset. However, we showcase that it is possible to reduce the number of unlabeled samples from the source distribution to compute the empirical mean and covariant matrix for PeTTA, without significantly impacting its performance.

D.5. Novelty of PeTTA

PeTTA is composed of multiple components. Among them, the anchor loss is an existing idea (examples of previous work utilizing this idea are [12, 31]). Similarly, the mean-teacher update; and regularization are well-established techniques and very useful for the continual or gradual TTA scenario. Hence, we do not aim to improve or alternate these components.

Nevertheless, the novelty of our contribution is the *sensing of the divergence and adaptive model update*, in which the importance of minimizing the loss (adaptation) and regularization (collapse prevention) is changed adaptively. In short, we propose a harmonic way of combining those elements adaptively to achieve a persistent TTA process.

The design of PeTTA draws inspiration from a theoretical analysis (Sec. 4.2), empirically surpassing both the conventional reset-based approach [43] (Appdx. E.3) and other continual TTA approaches [7, 12, 22, 56, 58] on our proposed recurring TTA (Sec. 4.1, Appdx. E.1), as well as the previously established CCC [43] benchmark (Appdx. E.4).

E. Additional Experimental Results of PeTTA

E.1. Performance of PeTTA Versus Compared Methods

Performance on CIFAR-100-C and Domainnet Datasets. Due to the length constraint, the classification errors on the tasks CIFAR-100 \rightarrow CIFAR-100-C, and *real* \rightarrow *clipart*, *painting*, *sketch* of DomainNet are provided in Tab. 6 and Tab. 7. To prevent model collapse, the adaptability of PeTTA is more constrained. As a result, it requires more time for adaptation initially (e.g., in the first visit) but remains stable thereafter. Generally, consistent trends and observations are identified across all four TTA tasks.

Table 6. Average classification error of the task CIFAR-100 \rightarrow CIFAR-100-C in *recurring TTA* scenario. The lowest error is highlighted in **bold**. (*) Average error across 5 runs (different random seeds) is reported for PeTTA.

Method	Recurring TTA visit \rightarrow																				Avg	
	1	2	3	4	5	6	7	8	9	10	11	12	13	14	15	16	17	18	19	20		
Source																					46.5	
LAME [7]																					40.5	
CoTTA [56]	53.4	58.4	63.4	67.6	71.4	74.9	78.2	81.1	84.0	86.7	88.8	90.7	92.3	93.5	94.7	95.6	96.3	97.0	97.3	97.6	83.1	
RMT [12]	50.5	48.6	47.9	47.4	47.3	47.1	46.9	46.9	46.6	46.8	46.7	46.5	46.5	46.6	46.5	46.5	46.5	46.5	46.5	46.5	46.5	47.1
MECTA [22]	44.8	44.3	44.6	43.1	44.8	44.2	44.4	43.8	43.8	43.9	44.6	43.8	44.4	44.6	43.9	44.2	43.8	44.4	44.9	44.2	44.2	44.2
RoTTA [58]	35.5	35.2	38.5	41.9	45.3	49.2	52.0	55.2	58.1	61.5	64.6	67.5	70.7	73.2	75.4	77.1	79.2	81.5	82.8	84.5	61.4	
RDumb [43]	36.7	36.7	36.6	36.6	36.7	36.8	36.7	36.5	36.6	36.5	36.7	36.6	36.5	36.7	36.5	36.6	36.6	36.6	36.7	36.6	36.5	36.6
PeTTA (ours)(*)	35.8	34.4	34.7	35.0	35.1	35.1	35.2	35.3	35.3	35.3	35.2	35.3	35.2	35.2	35.2	35.1	35.2	35.2	35.2	35.2	35.2	35.1

Table 7. Average classification error of the task *real* \rightarrow *clipart* \rightarrow *painting* \rightarrow *sketch* on DomainNet dataset in *recurring TTA* scenario.

Method	Episodic TTA visit \longrightarrow																				Avg
	1	2	3	4	5	6	7	8	9	10	11	12	13	14	15	16	17	18	19	20	
Source																					45.3
LAME [7]																					45.6
CoTTA [56]	96.2	97.1	97.4	97.8	98.1	98.2	98.4	98.4	98.4	98.5	98.6	98.6	98.6	98.6	98.6	98.7	98.7	98.7	98.7	98.7	98.3
RMT [12]	76.2	77.1	77.3	77.3	77.2	77.1	76.8	76.9	76.5	76.4	76.4	76.3	76.4	76.2	76.2	76.1	76.4	76.1	76.0	75.8	76.5
MECTA [22]	94.6	98.4	98.6	98.8	99.1	99.0	99.0	99.0	99.0	99.0	99.0	99.0	99.0	99.0	99.0	99.0	99.0	99.0	99.0	99.0	98.7
RoTTA [58]	44.3	43.8	44.7	46.7	48.7	50.8	52.7	55.0	57.1	59.7	62.7	65.1	68.0	70.3	72.7	75.2	77.2	79.6	82.6	85.3	62.1
RDumb [43]	44.3	44.4	44.3	44.5	44.2	44.2	44.3	44.5	44.4	44.2	44.3	44.3	44.3	44.3	44.5	44.3	44.2	44.3	44.4	44.3	44.3
PeTTA (ours) ^(*)	43.8	42.6	42.3	42.3	42.6	42.8	42.8	43.0	42.9	42.9	43.1	43.0	42.9	43.0	43.0	43.1	43.0	42.8	42.9	42.9	42.9

Standard Deviation of PeTTA Performance Across Multiple Runs. For PeTTA experiments marked with (*) in Tab. 1, Tab. 2, Tab. 6, and Tab. 7, the average performance across five independent runs with different random seeds is reported. Due to the space constraint, the corresponding standard deviation values are now reported in Tab. 8. Generally, the average standard deviation across runs stays within $\pm 0.1\%$ for small datasets (CIFAR-10-C, CIFAR-100-C) and $\pm 0.5\%$ for larger datasets (ImageNet-C, DomainNet).

Table 8. Mean and standard deviation classification error of PeTTA on the four datasets: CIFAR-10-C (CF-10-C), CIFAR-100-C (CF-100-C), DomainNet (DN), and ImageNet-C (IN-C) with *recurring TTA* scenario. Each experiment is run 5 times with 5 random seeds.

Dataset	Recurring TTA visit \longrightarrow																				Avg
	1	2	3	4	5	6	7	8	9	10	11	12	13	14	15	16	17	18	19	20	
CF-10-C	24.3	23.0	22.6	22.4	22.4	22.5	22.3	22.5	22.8	22.8	22.6	22.7	22.7	22.9	22.6	22.7	22.6	22.8	22.9	23.0	22.8
	± 0.4	± 0.3	± 0.4	± 0.3	± 0.3	± 0.3	± 0.4	± 0.2	± 0.3	± 0.4	± 0.4	± 0.2	± 0.1	± 0.3	± 0.5	± 0.2	± 0.2	± 0.3	± 0.4	± 0.5	± 0.1
CF-100-C	35.8	34.4	34.7	35.0	35.1	35.1	35.2	35.3	35.3	35.3	35.2	35.3	35.2	35.1	35.2	35.2	35.2	35.2	35.2	35.2	35.1
	± 0.4	± 0.4	± 0.2	± 0.2	± 0.1	± 0.1	± 0.2	± 0.2	± 0.1	± 0.2	± 0.1	± 0.2	± 0.2	± 0.1	± 0.1	± 0.1	± 0.1	± 0.1	± 0.1	± 0.2	± 0.1
DN	43.8	42.6	42.3	42.3	42.6	42.8	42.8	43.0	42.9	42.9	43.1	43.0	42.9	43.0	43.0	43.1	43.0	42.8	42.9	42.9	42.9
	± 0.1	± 0.1	± 0.2	± 0.2	± 0.3	± 0.3	± 0.3	± 0.4	± 0.4	± 0.4	± 0.4	± 0.4	± 0.4	± 0.3	± 0.3	± 0.2	± 0.4	± 0.3	± 0.3	± 0.3	± 0.3
IN-C	65.3	61.7	59.8	59.1	59.4	59.6	59.8	59.3	59.4	60.0	60.3	61.0	60.7	60.4	60.6	60.7	60.8	60.7	60.4	60.2	60.5
	± 0.6	± 0.5	± 0.5	± 0.5	± 1.4	± 1.1	± 1.0	± 0.5	± 0.8	± 0.9	± 0.4	± 0.8	± 0.9	± 0.8	± 0.9	± 0.8	± 1.0	± 0.6	± 0.6	± 0.7	± 0.5

E.2. An Inspection of PeTTA

In Fig. 6, we showcase an inspection of our PeTTA on the task CIFAR-10 \rightarrow CIFAR-10-C [19] in a typical recurring TTA with 20 visits. Specifically, the visualizations of PeTTA parameters ($\bar{\gamma}_t$, λ_t , and α_t), adaptation losses (\mathcal{L}_{CLS} , \mathcal{L}_{AL}) and regularization term ($\mathcal{R}(\theta)$) are provided. Here, we observe the values of adaptive parameters λ_t and α_t continuously changing through time, as the testing scenarios evolve during recurring TTA. This proposed mechanism *stabilizes* the value of the loss functions, and regularization term, balancing between the two primary objectives: adaptation and preventing model collapse. Thus, *the error rate persists* as a result. A similar pattern is observed on other datasets (CIFAR-100-C [19] and DomainNet [42]).

E.3. Does Model Reset Help?

Experiment Setup. We use the term “*model reset*” to represent the action of “*reverting the current TTA model to the source model*”. This straightforward approach is named RDumb [43]. We thoroughly conducted experiments to compare the performance of RDumb with PeTTA. The implementation of RDumb in this setting is as follows. We employ RoTTA [58] as the base test-time adaptor due to the characteristics of the practical TTA [58] stream. The model (*including model parameters, the optimizer state, and the memory bank*) is reset after adapting itself to T images.¹ For each dataset, three values of this hyper-parameter T are selected:

- $T = 1,000$: This is the value selected by the RDumb’s authors [43]. Unless specifically stated, we use this value when reporting the performance of RDumb [43] in all other tables.

¹A slight abuse of notation. T here is the number of images between two consecutive resets, following the notation on Sec. 3 of [43], *not* the sample indices in our notations.

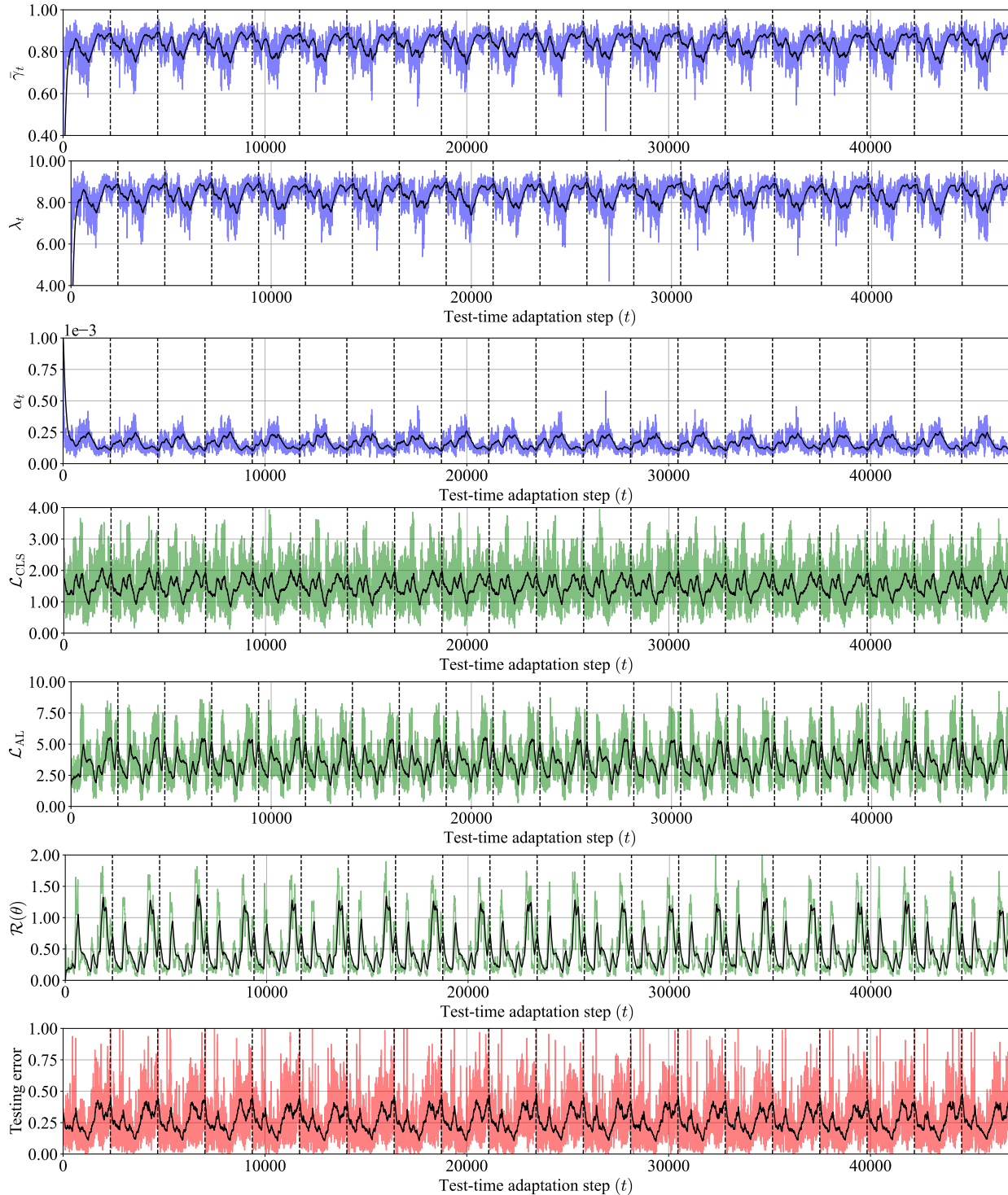


Figure 6. An inspection of PeTTA on the task CIFAR-10 \rightarrow CIFAR-10-C [19] in a recurring with 20 visits (visits are separated by the vertical dashed lines). Here, we visualize (rows 1-3) the dynamic of PeTTA adaptive parameters ($\tilde{\gamma}_t, \lambda_t, \alpha_t$), (rows 4-5) the value of the loss functions ($\mathcal{L}_{CLS}, \mathcal{L}_{AL}$) and (row 6) the value of the regularization term ($\mathcal{R}(\theta)$) and (row 7) the classification error rate at each step. The solid line in the foreground of each plot denotes the running mean. The plots show an adaptive change of λ_t, α_t through time in PeTTA, which stabilizes TTA performance, making PeTTA achieve a persisting adaptation process in all observed values across 20 visits.

- $T = 10,000$ (CIFAR-10/100-C), $T = 5,000$ (ImageNet-C) and $T = 24,237$ (DomainNet).² This value is equal to the number of samples in the test set of a *single corruption type*, i.e., the model is reset exactly after visiting each \mathcal{P}_i 's (see Sec. 4.1 for notations). For DomainNet [42], since the number of images within each domain is unequal, the average number of images is used instead.
- $T = 150,000$ (CIFAR-10/100-C), $T = 75,000$ (ImageNet-C) and $T = 72,712$ (DomainNet). This number is equal to the number of samples *in one recurrence* of our recurring TTA, i.e., the model is reset exactly after visiting $\mathcal{P}_1 \rightarrow \dots \rightarrow \mathcal{P}_D$. Here, $D = 15$ - types of corruptions [19] for CIFAR-10/100-C and ImageNet-C and $D = 3$ for DomainNet (*clipart, painting, sketch*). For example, the model is reset 20 times within a *recurring TTA* setting with 20 recurrences under this choice of T .

The second and the last reset scheme could be interpreted as assuming the model has access to *an oracle model* with a capability of signaling the transitions between domains, or recurrences. Typically, this is *an unrealistic capability in real-world scenarios*, and a desirable continual TTA algorithm should be able to operate independently without knowing when the domain shift happening.

Experimental Results. An empirical comparison between RDumb [43] and our PeTTA are reported in Tab. 9, Tab. 10, Tab. 11 and Tab. 12 for all four tasks.

Table 9. Average classification error comparison between RDumb [43] (a reset-based approach) with different reset frequencies and our PeTTA on CIFAR-10 \rightarrow CIFAR-10-C task.

Reset Every	Recurring TTA visit \longrightarrow																				Avg
	1	2	3	4	5	6	7	8	9	10	11	12	13	14	15	16	17	18	19	20	
$T = 1000$	31.1	32.1	32.3	31.6	31.9	31.8	31.8	31.9	31.9	32.1	31.7	32.0	32.5	32.0	31.9	31.6	31.9	31.4	32.3	32.4	31.9
$T = 10000$	25.8	25.9	26.5	26.1	26.4	25.4	25.8	25.8	26.1	26.2	26.1	26.1	26.1	26.1	25.9	25.5	25.5	25.7	26.2	26.0	26.0
$T = 150000$	24.8	25.3	24.3	24.1	25.3	25.4	25.4	24.5	25.0	24.9	25.0	24.8	25.0	24.5	24.9	24.1	24.0	24.7	24.9	24.4	24.8
PeTTA (ours) ^(*)	24.3	23.0	22.6	22.4	22.4	22.5	22.3	22.5	22.8	22.8	22.6	22.7	22.7	22.9	22.6	22.7	22.6	22.8	22.9	23.0	22.8

Table 10. Average classification error comparison between RDumb [43] (a reset-based approach) with different reset frequencies and our PeTTA on CIFAR-100-C dataset.

Reset Every	Recurring TTA visit \longrightarrow																				Avg
	1	2	3	4	5	6	7	8	9	10	11	12	13	14	15	16	17	18	19	20	
$T = 1000$	36.7	36.7	36.6	36.6	36.7	36.8	36.7	36.5	36.6	36.5	36.7	36.6	36.5	36.7	36.5	36.6	36.6	36.7	36.6	36.5	36.6
$T = 10000$	43.5	43.6	43.7	43.7	43.4	43.5	43.6	43.4	43.5	43.6	43.8	43.5	43.5	43.6	43.4	43.6	43.5	43.8	43.7	43.6	43.6
$T = 150000$	35.4	35.4	35.4	35.3	35.4	35.4	35.5	35.6	35.4	35.4	35.5	35.3	35.2	35.4	35.1	35.8	35.1	35.6	35.3	35.8	35.4
PeTTA (ours) ^(*)	35.8	34.4	34.7	35.0	35.1	35.1	35.2	35.3	35.3	35.3	35.2	35.3	35.2	35.2	35.1	35.2	35.2	35.2	35.2	35.2	35.1

Table 11. Average classification error comparison between RDumb [43] (a reset-based approach) with different reset frequencies and our PeTTA on DomainNet dataset.

Reset Every	Recurring TTA visit \longrightarrow																				Avg
	1	2	3	4	5	6	7	8	9	10	11	12	13	14	15	16	17	18	19	20	
$T = 1000$	44.3	44.4	44.3	44.5	44.2	44.2	44.3	44.5	44.4	44.2	44.3	44.3	44.3	44.3	44.5	44.3	44.2	44.3	44.4	44.3	44.3
$T = 24237$	44.1	44.3	43.9	44.2	44.1	44.3	44.2	44.4	44.1	44.1	44.0	44.3	44.1	44.0	44.0	44.2	44.1	44.1	44.1	44.4	44.1
$T = 72712$	44.3	44.3	44.0	44.3	44.1	44.3	44.2	44.4	44.2	44.1	44.0	44.1	44.2	44.1	44.1	44.1	44.1	44.0	44.0	44.3	44.2
PeTTA (ours) ^(*)	43.8	42.6	42.3	42.3	42.6	42.8	42.8	43.0	42.9	42.9	43.1	43.0	42.9	43.0	43.0	43.1	43.0	42.8	42.9	42.9	42.9

Discussions. Across datasets and reset frequencies, our PeTTA approach is always *better* than RDumb [43]. The supreme performance holds even when RDumb has access to the oracle information that can reset the model exactly at the transition between each domain shift or recurrence. Importantly, this oracle information is typically unavailable in practice.

Noteworthy, it is clear that the performance of RDumb varies when changing the choice of the reset frequency. For a given choice of T , the better performance on one dataset does not guarantee the same performance on other datasets. For example, $T = 1,000$ - the best empirical value found by RDumb authors [43] on CCC, does not give the best performance on our recurring TTA scenario; the second choice of T negatively impact the performance on many tasks; the third choice

²A subset of 5,000 samples from ImageNet-C are selected following RobustBench [10] for a consistent evaluation with other benchmarks.

Table 12. Average classification error comparison between RDumb [43] (a reset-based approach) with different reset frequencies and our PeTTA on ImageNet-C dataset.

Reset Every	Recurring TTA visit \longrightarrow																				Avg
	1	2	3	4	5	6	7	8	9	10	11	12	13	14	15	16	17	18	19	20	
$T = 1000$	72.2	73.0	73.2	72.8	72.2	72.8	73.3	72.7	71.9	73.0	73.2	73.1	72.0	72.7	73.3	73.1	72.1	72.6	73.3	73.1	72.8
$T = 5000$	70.2	70.8	71.6	72.1	72.4	72.6	72.9	73.1	73.2	73.6	73.7	73.9	74.0	74.0	74.3	74.1	74.1	73.8	73.5	71.9	73.0
$T = 75000$	67.0	67.1	67.2	67.5	67.5	67.6	67.8	67.6	67.6	67.6	67.5	67.7	67.6	67.9	68.1	67.9	67.4	67.5	67.7	67.5	67.6
PeTTA (ours) ^(*)	65.3	61.7	59.8	59.1	59.4	59.6	59.8	59.3	59.4	60.0	60.3	61.0	60.7	60.4	60.6	60.7	60.8	60.7	60.4	60.2	60.5

gives the best results, but knowing this exact recurrence frequency of the testing stream is unrealistic. The result highlights the challenge in practice when tuning this parameter (too slow/frequent), especially in the TTA setting where a validation set is unavailable. Our PeTTA, in contrast, is reset-free.

E.4. PeTTA with Continuously Changing Corruption (CCC) Setting

Experiment Setup. In this section, we further evaluate the performance of our PeTTA on the testing data stream of Continuous Changing Corruption (CCC) [43] setting. Here we use the baseline accuracy 20%, transition speed 1000, and random seed 44.³ The compared methods are source model (ResNet 50), PeTTA, RoTTA [58], and RDumb [43]. Noteworthy, different from recurring TTA, the class labels here are i.i.d. distributed. The adaptation configuration of PeTTA follows the same settings as used on ImageNet-C, while the same setting introduced in Sec. E.3, with $T = 1000$ is used for RDumb [43].

Experimental Results. The classification errors of all approaches on CCC [43] are provided in Tab. 13. Here, we present the average classification error between two consecutive adaptation step intervals. An adaptation step in this table corresponds to a mini-batch of data with 64 images. The model is adapted to 80,000 steps in total with more than 5.1M images.

Table 13. Average classification error on CCC [43] setting. Each column presents the average error within an adaptation interval (e.g., the second column provides the average error between the 6701 and 13400 adaptation steps). Each adaptation step here is performed on a mini-batch of 64 images.

Method	CCC [43] Adaptation Step \longrightarrow												Avg
	6700	13400	20100	26800	33500	40200	46900	53600	60200	66800	73400	80000	
Source	0.83	0.83	0.83	0.83	0.83	0.84	0.84	0.83	0.84	0.83	0.83	0.83	0.83
RoTTA [58]	0.70	0.85	0.92	0.96	0.98	1.00	1.00	1.00	1.00	1.00	1.00	1.00	0.95
RDumb [43]	0.78	0.74	0.75	0.77	0.75	0.72	0.75	0.77	0.75	0.74	0.75	0.75	0.75
PeTTA (ours)	0.67	0.63	0.62	0.65	0.65	0.64	0.64	0.68	0.63	0.63	0.65	0.65	0.64

Discussions. Under the CCC [43] setting, we demonstrate the advantage of using our PeTTA over the source model, RoTTA [58] and a reset-based approach RDumb [43]. The lifelong performance degradation is also observed on RoTTA [58], as its performance matches PeTTA at the beginning but quickly collapses afterward.

The result here not only further validates PeTTA on an external setting of lifelong performance degradation but also empirically justifies the construction of our recurring TTA as a diagnostic tool (Appdx. C.2) where similar observations are concluded on the two settings. Obviously, our recurring TTA is notably simpler than CCC [43].

E.5. More Details on the Ablation Study

We provide the detailed classification error for each visit in the recurring TTA setting of each row entry in Tab. 3 (PeTTA Ablation Study): Tab. 14, Tab. 15, Tab. 16, Tab. 17; and Tab. 4 (PeTTA with various choices of regularizers): Tab. 18, Tab. 19, Tab. 20, Tab. 21.

Fig. 7 presents an additional examination of the ablation study conducted on the task CIFAR-100 \rightarrow CIFAR-100-C [19] for our PeTTA approach. We plot the classification error (top) and the value of $\bar{\gamma}_t$ (bottom) for various PeTTA variations. As the model diverges from the initial state, the value of $\bar{\gamma}_t$ increases. Unable to adjust α_t or constraint the probability space via \mathcal{L}_{AL} limits the ability of PeTTA to prevent model collapse. In all variations with the model collapse in ablation studies, the rapid saturation of $\bar{\gamma}_t$ is all observed. Therefore, incorporating all components in PeTTA is necessary.

³<https://github.com/oripress/CCC>

Table 14. Average classification error of multiple variations of PeTTA. Experiments on CIFAR10 \rightarrow CIFAR10-C [19] task.

Method	Episodic TTA visit \longrightarrow																				Avg
	1	2	3	4	5	6	7	8	9	10	11	12	13	14	15	16	17	18	19	20	
Baseline w/o $\mathcal{R}(\theta)$	23.5	24.0	27.4	29.9	33.4	35.6	38.0	40.7	43.1	45.0	46.0	48.6	50.0	49.7	50.8	51.5	52.3	53.3	54.3	55.5	42.6
$\mathcal{R}(\theta)$ fixed $\lambda = 0.1\lambda_0$	23.5	24.0	27.2	29.8	33.4	35.3	37.9	40.5	43.3	45.3	46.8	49.3	50.9	51.0	52.1	53.2	54.0	54.8	56.0	57.6	43.3
$\mathcal{R}(\theta)$ fixed $\lambda = \lambda_0$	23.5	23.6	26.2	28.4	31.6	33.5	36.4	38.7	41.1	43.1	44.8	47.6	49.3	49.5	50.9	52.1	53.1	54.2	55.6	57.0	42.0
PeTTA- λ_t	24.9	25.3	26.0	26.4	27.2	26.5	27.2	27.1	27.4	27.7	27.8	28.0	27.5	28.0	27.7	27.4	27.0	27.6	27.8	27.8	27.1
PeTTA- $\lambda_t + \alpha_t$	25.5	24.5	23.7	23.1	23.2	22.4	23.3	23.2	23.7	24.1	23.9	24.5	24.3	24.0	23.8	23.9	23.8	24.1	24.6	24.7	23.9
PeTTA- $\lambda_t + \mathcal{L}_{AL}$	23.3	23.9	24.6	25.3	26.2	25.9	26.4	26.6	26.9	26.6	26.7	26.7	26.8	26.8	27.2	26.9	26.9	26.8	27.0	26.2	26.2
PeTTA $\alpha_t + \mathcal{L}_{AL}$	24.3	23.0	22.6	22.4	22.4	22.5	22.3	22.5	22.8	22.8	22.6	22.7	22.7	22.9	22.6	22.7	22.6	22.8	22.9	23.0	22.8

Table 15. Average classification error of multiple variations of PeTTA. Experiments on CIFAR-100 \rightarrow CIFAR100-C [19] task.

Method	Episodic TTA visit \longrightarrow																				Avg
	1	2	3	4	5	6	7	8	9	10	11	12	13	14	15	16	17	18	19	20	
Baseline w/o $\mathcal{R}(\theta)$	40.2	46.3	51.2	54.4	57.3	59.4	61.3	62.6	63.9	65.1	66.3	67.1	68.1	68.9	69.6	70.3	71.1	71.6	72.4	72.9	63.0
$\mathcal{R}(\theta)$ fixed $\lambda = 0.1\lambda_0$	40.5	46.1	51.5	55.1	58.2	60.5	62.6	64.2	65.7	67.3	68.6	69.5	70.6	71.6	72.5	73.4	74.2	74.9	75.8	76.5	65.0
$\mathcal{R}(\theta)$ fixed $\lambda = \lambda_0$	41.8	47.6	52.6	56.1	58.9	60.7	62.5	63.9	65.0	66.2	67.1	68.3	69.5	70.3	71.4	72.4	73.4	74.1	75.0	75.6	64.6
PeTTA- λ_t	39.4	43.4	46.6	49.1	51.0	52.6	53.8	54.7	55.7	56.5	57.1	57.7	58.3	58.8	59.3	59.9	60.6	61.0	61.6	62.1	55.0
PeTTA- $\lambda_t + \alpha_t$	39.4	40.1	40.8	40.7	41.2	41.5	41.4	41.6	41.5	41.5	41.7	41.6	41.8	41.7	41.8	42.0	41.9	41.9	42.0	41.8	41.4
PeTTA- $\lambda_t + \mathcal{L}_{AL}$	36.2	35.6	35.7	36.1	36.2	36.4	36.4	36.5	36.2	36.2	36.6	36.5	36.5	36.6	36.5	36.6	36.5	36.6	36.5	36.3	36.3
PeTTA $\lambda_t + \alpha_t + \mathcal{L}_{AL}$	35.8	34.4	34.7	35.0	35.1	35.1	35.2	35.3	35.3	35.3	35.2	35.3	35.2	35.2	35.1	35.2	35.2	35.2	35.2	35.2	35.1

Table 16. Average classification error of multiple variations of PeTTA. Experiments on *real* \rightarrow *clipart*, *painting*, *sketch* task from DomainNet [42] task.

Method	Recurring TTA visit \longrightarrow																				Avg
	1	2	3	4	5	6	7	8	9	10	11	12	13	14	15	16	17	18	19	20	
Baseline w/o $\mathcal{R}(\theta)$	52.3	69.0	68.6	68.6	69.4	70.5	71.8	73.4	75.6	77.6	78.8	81.0	82.8	84.3	85.9	87.4	88.5	89.9	90.8	92.1	77.9
$\mathcal{R}(\theta)$ fixed $\lambda = 0.1\lambda_0$	52.5	70.0	69.8	70.0	71.1	72.5	74.6	76.1	77.8	80.4	81.9	83.5	85.2	87.2	89.1	90.2	91.5	93.2	94.1	94.9	80.0
$\mathcal{R}(\theta)$ fixed $\lambda = \lambda_0$	54.6	69.8	63.7	56.0	61.7	76.4	70.4	62.5	58.2	76.0	73.6	66.8	58.6	62.3	80.8	75.5	67.0	59.9	59.3	78.3	66.6
PeTTA- λ_t	49.2	64.5	62.4	60.9	59.6	58.6	57.7	57.8	57.6	57.7	58.0	58.5	59.0	59.5	59.8	61.1	62.0	62.6	63.6	64.9	59.7
PeTTA- $\lambda_t + \alpha_t$	43.9	42.5	42.3	42.3	42.6	42.8	43.1	43.7	43.9	44.3	44.6	45.1	45.4	45.7	45.7	46.1	46.1	46.2	46.5	46.4	44.5
PeTTA- $\lambda_t + \mathcal{L}_{AL}$	43.6	42.5	42.6	42.6	42.9	43.0	43.3	43.4	43.1	43.2	43.1	43.3	43.3	43.2	43.2	43.9	43.7	43.0	43.2	43.5	43.2
PeTTA $\lambda_t + \alpha_t + \mathcal{L}_{AL}$	43.8	42.6	42.3	42.3	42.6	42.8	42.8	43.0	42.9	42.9	43.1	43.0	42.9	43.0	43.0	43.1	43.0	42.8	42.9	42.9	42.9

Table 17. Average classification error of multiple variations of PeTTA. Experiments on ImageNet \rightarrow ImageNet-C [19] task.

Method	Recurring TTA visit \longrightarrow																				Avg
	1	2	3	4	5	6	7	8	9	10	11	12	13	14	15	16	17	18	19	20	
Baseline w/o $\mathcal{R}(\theta)$	66.9	61.9	72.7	93.6	97.4	97.8	98.0	98.2	98.3	98.3	98.4	98.4	98.5	98.5	98.6	98.6	98.6	98.6	98.7	98.7	93.4
$\mathcal{R}(\theta)$ fixed $\lambda = 0.1\lambda_0$	65.5	70.9	79.1	85.2	90.3	92.6	95.8	95.8	95.4	97.3	96.9	97.7	97.9	98.2	98.0	98.7	98.6	98.4	98.4	98.7	92.5
$\mathcal{R}(\theta)$ fixed $\lambda = \lambda_0$	66.5	62.1	73.0	93.5	97.0	97.2	97.5	97.5	97.6	97.5	97.7	97.7	97.7	97.7	97.9	97.9	98.0	98.0	98.0	97.9	92.9
PeTTA- λ_t	65.9	62.1	76.3	96.7	97.0	96.9	96.9	96.9	97.0	97.1	97.0	97.2	97.0	97.1	97.1	97.0	97.0	97.0	97.0	97.0	92.7
PeTTA- $\lambda_t + \alpha_t$	64.8	70.5	74.6	75.8	75.5	75.8	76.1	76.2	76.2	76.5	76.7	77.0	76.9	77.4	77.1	77.3	77.2	77.4	77.6	77.4	75.7
PeTTA- $\lambda_t + \mathcal{L}_{AL}$	64.8	61.1	60.0	59.8	60.4	60.4	61.2	61.2	61.8	61.9	62.1	62.2	62.1	62.9	62.1	62.8	62.7	62.1	62.8	66.6	62.0
PeTTA (<i>ours</i>) ^(*)	65.3	61.7	59.8	59.1	59.4	59.6	59.8	59.3	59.4	60.0	60.3	61.0	60.7	60.4	60.6	60.7	60.8	60.7	60.4	60.2	60.5

Table 18. Average classification error of PeTTA with various choices of regularizers. Experiments on CIFAR-10 \rightarrow CIFAR-10-C [19] task.

Method	Episodic TTA visit \longrightarrow																				Avg
	1	2	3	4	5	6	7	8	9	10	11	12	13	14	15	16	17	18	19	20	
L2	25.6	24.8	23.8	23.1	23.2	22.7	23.0	22.7	22.7	22.7	22.8	22.7	22.8	22.7	22.5	22.3	22.2	22.4	22.7	22.8	23.0
L2+Fisher	25.2	23.7	22.5	21.8	22.3	21.5	22.3	22.1	22.5	22.8	22.6	22.6	22.6	22.8	22.6	22.9	22.6	22.9	23.0	23.3	22.7
Cosine	24.3	23.0	22.6	22.4	22.4	22.5	22.3	22.5	22.8	22.6	22.7	22.7	22.7	22.9	22.6	22.7	22.6	22.8	22.9	23.0	22.8
Cosine+Fisher	25.1	23.8	22.2	21.6	22.0	21.4	22.0	21.8	22.1	22.3	22.5	22.4	22.6	22.6	22.4	22.7	22.6	22.8	22.8	23.3	22.6

Table 19. Average classification error of PeTTA with various choices of regularizers. Experiments on CIFAR-100 \rightarrow CIFAR-100-C [19] task.

Method	Recurring TTA visit \longrightarrow																				Avg
	1	2	3	4	5	6	7	8	9	10	11	12	13	14	15	16	17	18	19	20	
L2	36.9	35.5	35.5	35.5	35.7	35.6	35.6	35.5	35.5	35.4	35.6	35.5	35.7	35.7	35.7	35.7	35.8	35.5	35.4	35.5	35.6
L2+Fisher	36.8	35.4	35.4	35.8	35.9	36.0	35.9	35.9	35.9	35.8	36.1	36.1	36.1	36.1	36.1	36.1	36.2	36.0	36.0	35.9	36.0
Cosine	35.8	34.4	34.7	35.0	35.1	35.1	35.2	35.3	35.3	35.3	35.2	35.3	35.2	35.2	35.1	35.2	35.2	35.2	35.2	35.2	35.1
Cosine+Fisher	36.7	35.2	35.5	35.6	35.9	35.9	36.1	36.0	36.0	35.9	36.0	36.0	36.0	36.1	36.0	36.0	35.9	35.9	35.9	36.0	35.9

Table 20. Average classification error of PeTTA with various choices of regularizers. Experiments on *real* \rightarrow *clipart*, *painting*, *sketch* task from DomainNet [42] dataset.

Method	Recurring TTA visit \longrightarrow																				Avg
	1	2	3	4	5	6	7	8	9	10	11	12	13	14	15	16	17	18	19	20	
L2	43.8	42.7	42.5	42.4	42.8	42.9	43.0	43.1	43.1	43.2	43.4	43.3	43.2	43.3	43.2	43.2	43.4	43.0	43.1	43.1	43.1
L2+Fisher	43.9	42.8	42.7	43.0	43.2	43.4	43.6	43.8	43.9	44.1	44.0	44.2	44.2	44.2	44.4	44.4	44.5	44.5	44.5	44.5	43.9
Cosine	43.8	42.6	42.3	42.3	42.6	42.8	42.8	43.0	42.9	42.9	43.1	43.0	42.9	43.0	43.0	43.1	43.0	42.8	42.9	42.9	42.9
Cosine+Fisher	43.7	42.5	42.5	42.6	42.9	43.2	43.2	43.5	43.4	43.5	43.4	43.5	43.4	43.6	43.5	43.5	43.4	43.5	43.3	43.4	43.3

Table 21. Average classification error of PeTTA with various choices of regularizers. Experiments on ImageNet \rightarrow ImageNet-C [19] task.

Method	Recurring TTA visit \longrightarrow																				Avg
	1	2	3	4	5	6	7	8	9	10	11	12	13	14	15	16	17	18	19	20	
L2	70.8	72.2	71.5	69.8	72.3	69.3	70.3	70.5	70.0	70.8	70.2	72.1	71.4	70.8	70.9	70.9	69.7	71.0	71.1	70.4	70.8
L2+Fisher	70.5	70.0	69.5	69.4	69.6	69.9	69.2	69.3	72.2	70.4	71.0	70.5	71.7	71.5	71.3	68.4	68.6	68.8	68.7	68.7	70.0
Cosine	65.3	61.7	59.8	59.1	59.4	59.6	59.8	59.3	59.4	60.0	60.3	61.0	60.7	60.4	60.6	60.7	60.8	60.7	60.4	60.2	60.5
Cosine+Fisher	65.1	61.7	60.9	61.2	61.9	62.6	62.8	63.2	64.2	63.4	64.3	64.4	63.9	64.3	65.8	65.5	64.9	65.0	65.2	65.2	63.8

E.6. More Confusion Matrices in Recurring TTA Setting

For the task CIFAR-10 \rightarrow CIFAR-10-C [19] in *recurring TTA* setting (with 20 visits), we additionally showcase the confusion matrix of RoTTA [58] (Fig. 8) and our proposed PeTTA (Fig. 9) at each visit. Our PeTTA persistently achieves competitive performance across 20 visits while RoTTA [58] gradually degrades.

F. Experimental Details

F.1. Computing Resources

A computer cluster equipped with an Intel(R) Core(TM) 3.80GHz i7-10700K CPU, 64 GB RAM, and one NVIDIA GeForce RTX 3090 GPU (24 GB VRAM) is used for our experiments.

F.2. Test-time Adaptation Methods

Pre-trained Model on Source Distribution. Following previous studies [12, 54, 56, 58], only the batch norm layers are updated. As stated in Sec. 6.2, RobustBench [10] and torchvision [34] provide pre-trained models trained on source distributions. Specifically, for ImageNet-C and DomainNet experiments, a ResNet50 model [17] pre-trained on ImageNet V2 (specifically, checkpoint ResNet50_Weights.IMAGENET1K_V2 of torchvision) is used. From RobustBench, the model with checkpoint Standard and Hendrycks2020AugMix_ResNeXt [20] are adopted for CIFAR10-C and CIFAR-100-C experiments, respectively. Lastly, experiments on DomainNet dataset utilize the checkpoint (best_real_2020) provided in AdaContrast [8] study.⁴

Optimizer. Without specifically stated, Adam [26] optimizer with learning rate equal $1e^{-3}$, and $\beta = (0.9, 0.999)$ is selected as a universal choice for all experiments.

More Details on PeTTA. Since designing the batch normalization layers, and the memory bank is not the key focus of PeTTA, we conveniently adopt the implementation of the Robust Batch Norm layer and the Category-balanced Sampling strategy using a memory bank introduced in RoTTA [58].

⁴<https://github.com/DianCh/AdaContrast>

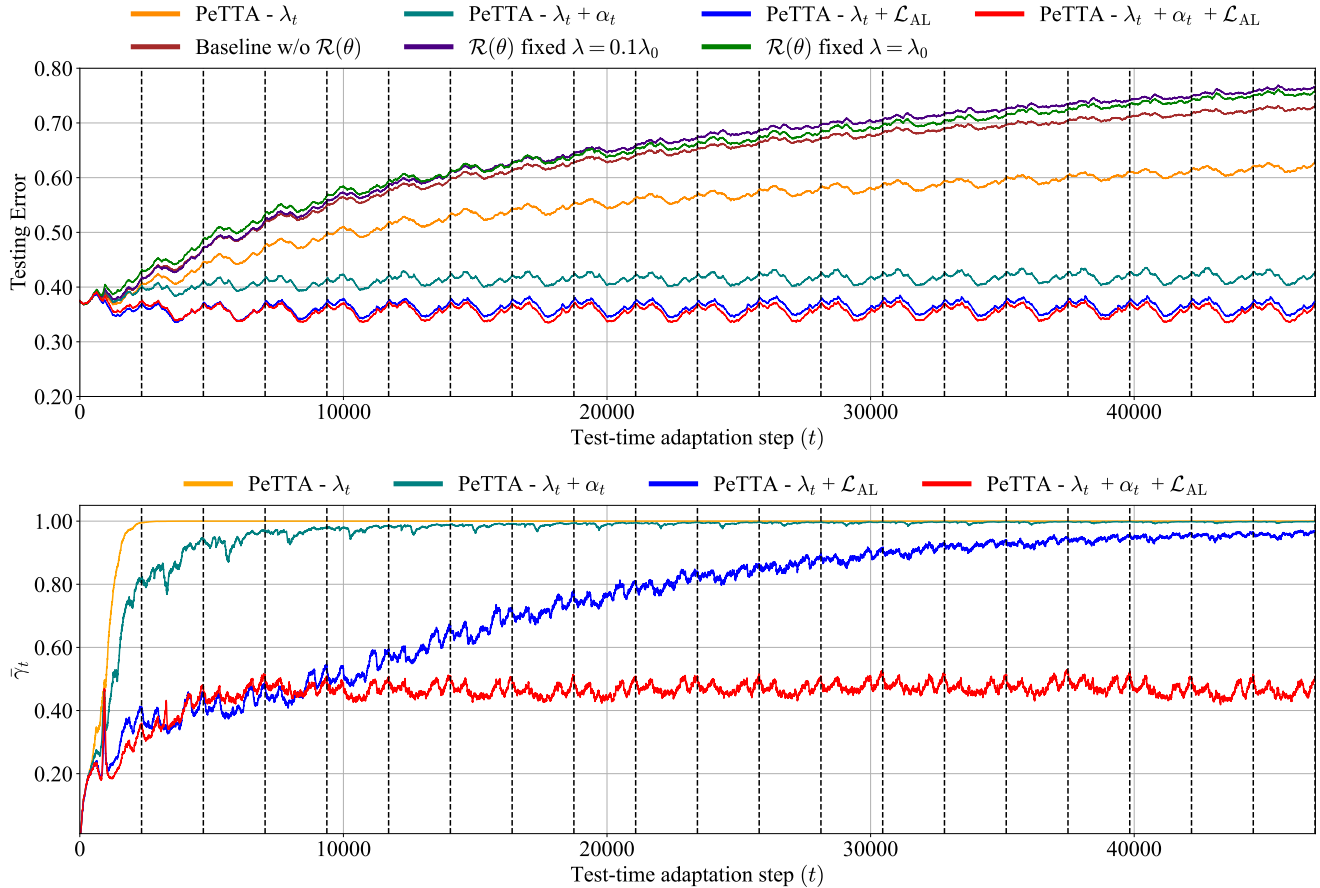


Figure 7. An inspection on the ablation study of multiple variations of PeTTA on the task CIFAR-100 \rightarrow CIFAR-100-C [19] in an episodic TTA with 20 visits (visits are separated by the vertical dashed lines). **(top)**: testing error of multiple variations of PeTTA. The performance of PeTTA without (w/o) $\mathcal{R}(\theta)$, or fixed regularization coefficient ($\lambda = \lambda_0/0.1\lambda_0$) degrades through time (the top 3 lines). The degradation of PeTTA $-\lambda_t$ is still happening but at a slower rate (justification below). The performance of the other three variations persists through time with PeTTA $-\lambda_t + \alpha_t + \mathcal{L}_{AL}$ achieves the best performance. **(bottom)**: changes of $\bar{\gamma}_t$ in multiple variations of PeTTA. When limiting the degree of freedom in adjusting α_t or lacking of supervision from \mathcal{L}_{AL} (e.g., PeTTA $-\lambda_t + \alpha_t$, PeTTA $-\lambda_t + \mathcal{L}_{AL}$, and especially PeTTA $-\lambda_t$), the value of $\bar{\gamma}_t$, unfortunately, escalates and eventually saturated. After this point, PeTTA has the same effect as using a fixed regularization coefficient. Therefore, fully utilizing all components is necessary to preserve the persistence of PeTTA. Best viewed in color.

F.3. The Use of Existing Assets

Many components of PeTTA is utilized from the official repository of RoTTA [58]⁵ and RMT [12].⁶ These two assets are released under MIT license. All the datasets, including CIFAR-10-C, CIFAR-100-C and ImageNet-C [19] are publicly available online, released under Apache-2.0 license.⁷ DomainNet dataset [42] (cleaned version) is also released for research purposes.⁸

⁵<https://github.com/BIT-DA/RoTTA>

⁶<https://github.com/mariodoebler/test-time-adaptation>

⁷<https://github.com/hendrycks/robustness>

⁸<https://ai.bu.edu/M3SDA/>

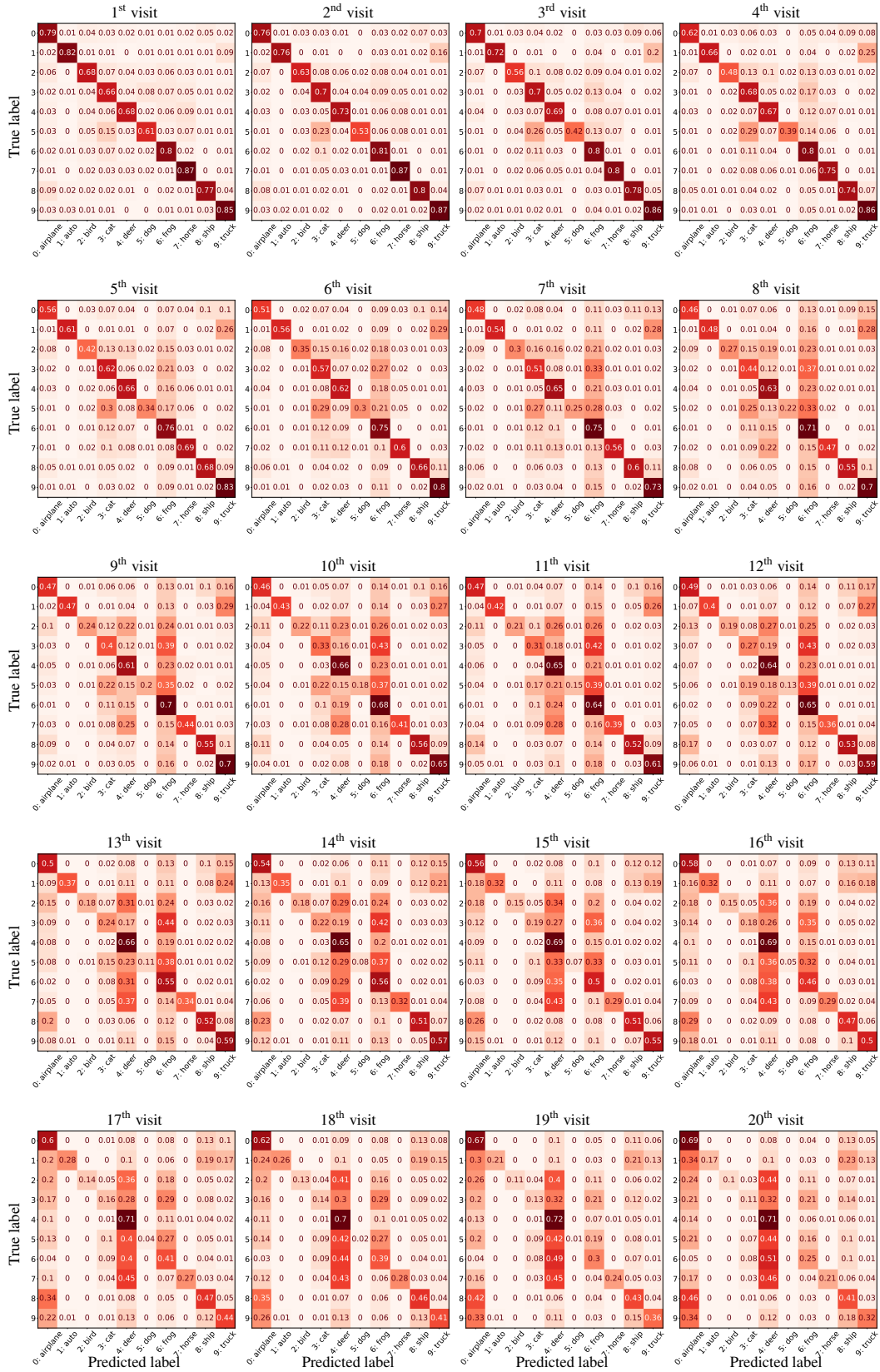


Figure 8. The dynamic of the confusion matrix of RoTTA [58] in episodic TTA with 20 visits.

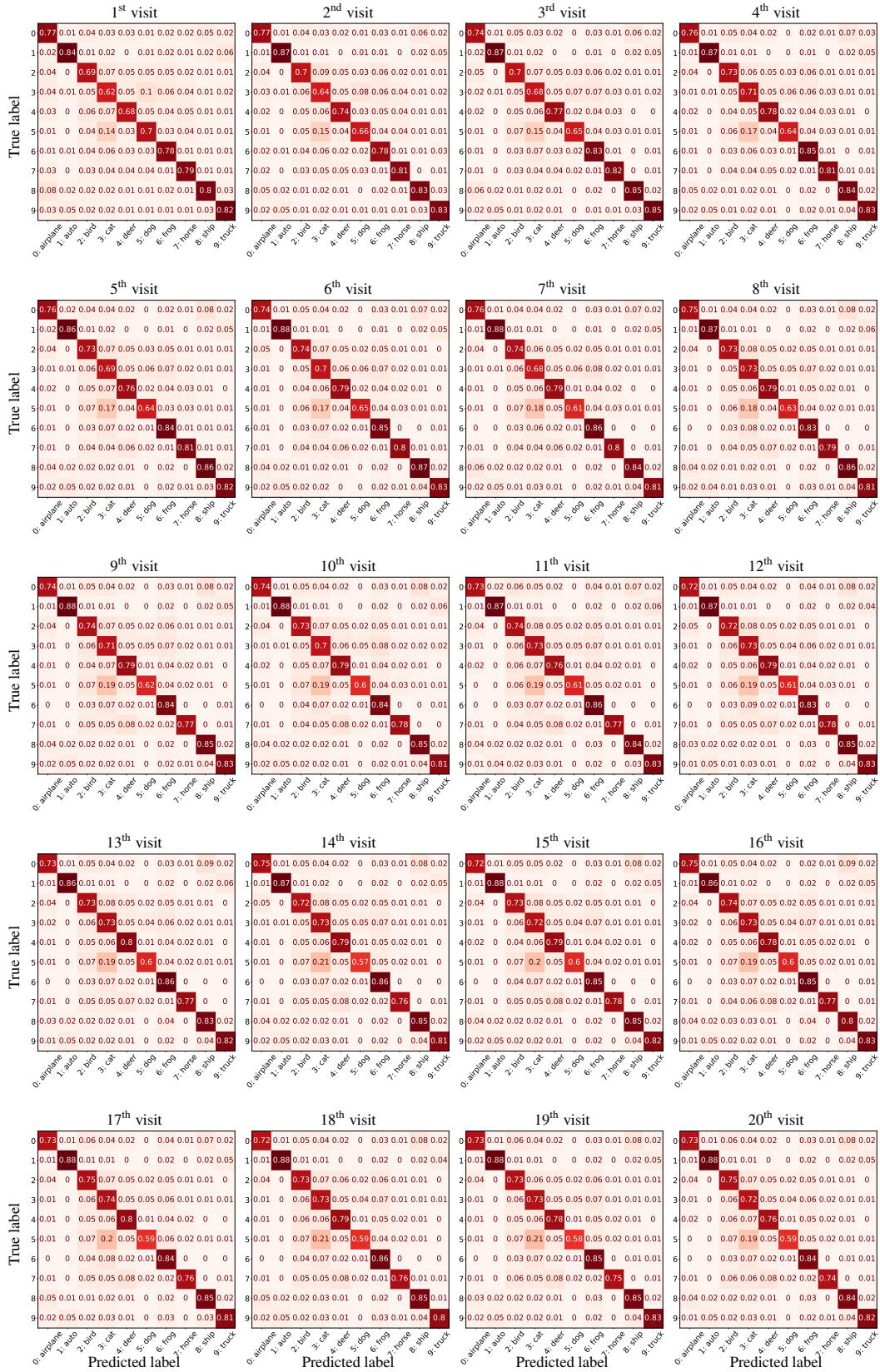


Figure 9. The dynamic of the confusion matrix of PeTTA (*ours*) in episodic TTA with 20 visits.